Resonance Raman Investigation of Protein Dynamics Studies on Myoglobin: Information Transmission and Energy Funneling Mechanisms

Ying Gao

Doctor of Philosophy

Department of Photoscience

School of Advanced Sciences

The Graduate University for Advanced Studies

2006

CONTENTS

Chapter 1. General Introduction

1.1. Heme proteins

Biological systems rely on heme-proteins to perform a number of basic functions essential for the survival, ranging from electron transfer, catalysis, oxygen transport and storage, electron transfer, regulation of kinase and control the gene expression. Hemes, or iron-porphyrin complexes, are the versatile prosthetic groups widely used in these proteins. Heme proteins have been the focus of a great deal of work over the last half a century and still retain a key place of interest in biochemical research. Heme proteins attracted special attention since the pioneering work on the structural determinations of myoglobin (Mb) and hemoglobin (Hb).

1.1.1. Myoglobin and Hemoglobin

The biological function of Mb is to buffer the oxygen concentration in the respiring tissues, wherein Hb, as the partner of Mb, releases oxygen to body tissues during its passage through respiring tissues, and transports the carbon dioxide to the opposite direction [1].

Sperm whale Mb and horse Hb A were the first protein of which the three-dimension crystal structures were solved with x-ray crystallography in 1960 [2,3]. The crystal structure of Mb is shown in Fig.1.1 [4]. Mb is comprised of eight α helices, which is labeled by A-H, and a hydrophobic pocket that stabilizes the binding of a single prosthetic group, iron protoporphyrin IX, which is designated as heme. The heme is embedded between E- and F-helices; the Fe atom is bound to the protein through the N_{ϵ} of F8 His (93) by a covalent bond and to a protoporphyrin through four pyrrole nitrogens. The crystal structure of Hb is shown in Fig.1.2 [5]. Hb is a tetramer consisting of two chemically identical heterodimers, each with an α- and a β-subunit. The α- and β-subunit has a globular structure, which is made up by all-α-helix in a packing way identical with the Mb [2,6]. Each subunit carries one heme. The α-subunit contains seven and the β-subunit contains eight helices. In a same way with Mb, the helices in

Hb have been named A through to H from the N- to C-termini, and interrupted by nonhelical segments AB, EF, FG and so on.

Mb and Hb can bind with ligands through Fe at the 6^{th}-coordination position (the only remaining coordination site) on the distal side of heme. In the Fe^{3+} (ferric, met, or oxidized) state, the heme can bind with a water molecule or different anions like N_3^-, CN^-, NO_2^-, SCN^- and F^-. In the Fe^{2+} (ferrous) state, the heme can bind with gaseous molecules, such as O_2, CO, and NO [1,7]. The binding of physiological ligand, O_2, with Mb is simple bimolecular reaction, but with Hb is cooperative[1]. Hb has two alternative quaternary structures in equilibrium, a tense structure (T) with low oxygen affinity, and a relaxed structure (R) with high oxygen affinity [8]. The deoxy state of Hb (deoxyHb) is predominantly in the T state, and the first dioxygen binds to deoxyHb with low affinity. However the binding of dioxygen stabilizes the R state, and thus the oxygen affinity increases with the number of bound oxygens. For both Mb and Hb, the iron atom is converted from high- (S=2) to low-spin (S=0) and moves into the porphyrin plane upon the transition from a deligated form to a ligated form (the distance from Fe to heme plane is about 0.3 Å in deoxyMb, and 0.5 Å in deoxyHb) [2,3]. In Hb, the presence and absence of the strains induced by the proximal histidine and the salt-bridges between the C-termini of the four subunits were thought be substantial for the transition between T- and R-states and the cooperativity between subunits [8,9]. The molecular mechanism of cooperativity in the oxygen binding of Hb leads us to understand the correlation between the function and structural changes. The large-amplitude motions at the quaternary level, which form a communication link at the subunit interface, are driven by changes in the tertiary structure upon ligation. In this respect, Mb that has a monomeric structure serves as a model system for the tertiary structural changes initiated by the binding or dissociation of a gaseous ligand.

1.1.2. Interaction between Heme and Protein in Myoglobin

There are four kinds of hemes utilized by the nature in the widely existing in heme proteins as shown in Fig.1.3A. The most common heme is *b* type heme or iron (II) protoporphyrin IX [10], whose ferric-hydroxy and ferric-chloride complexes are referred to as hemin. Heme *b*, also called protoheme, was found in *b* type cytochromes, globins and cytochromes P450, and heme-sensor proteins. Hemes *a* and *c* are biosynthetically derived [11-13]. Heme *a* is found only in terminal oxidases such as mammalian cytochromes *c* oxidase [12]. Heme *c* is found in cytochromes *c* as well as cytochrome *f* [14-17]. Heme *d* is the less common heme and found in the *Penicillium vitale* catalase [18]. The heme treated in this thesis mainly refers to heme *b*.

Protoheme exists as a prosthetic group of heme proteins which can bind with a gaseous ligand reversibly. As shown in Fig.1.3B, its framework is composed of a porphin ring with a Fe atom in the center, and as peripheral substituents of porphyrin ring methyl groups exist at 1, 3, 5 and 8 positions, vinyl groups exist at 2 and 4 positions and two propionate side chains exist at 7 and 8 positions. The heme is embedded in a hydrophobic pocket which is formed by the folding of helices. In Mb and Hb, the two propionate side chains are directed towards the complete reverse directions relative to the porphyrin plane and interact with surrounding residues in the heme pocket. There are several kinds of contacts between the heme and protein [19,20], for example, hydrophobic contacts between peripheral alkyl group and non-polar amino acid residues, coordination of His93 to the iron atom, and electrostatic interactions between two heme-propionate side chains, protruding into the solvent, and the polar residues, such as Arg45, Ser92 and His97 in Mb or His45α and Lys66β in Hb [21,22]. Propionate side chains have been found to be involved in regulating electron delivery to the iron center in some heme enzymes which are involved in electron transfers, like cytochromes and peroxidases. On the other hand, in some newly discovered heme-based sensor proteins, the propionate side

chains also were found to be responsible for the ligand recognition as well as regulation of conformational changes which is essential for signal transduction to the functional domain [23].

1.1.3. Ligand discrimination in Myoglobin

The typical functions of Mb are the storage and transport the O_2 in the muscle tissues of vertebrates. Consistent with this function, Mb exhibits a low rate of autoxidation and a high affinity for O_2 (P_{50} value of about 1μM) [24,25]. However, CO binds to Mb with an affinity that is 100 times higher than that of O_2 and even NO affinity is 10^5 times higher [25-28]. Although O_2 is the most abundant of these three gaseous ligands, it somehow appears incongruous for an O_2-binding protein. It becomes more reasonable after we compare the partition constant, defined as the ratio of equilibrium association constants for CO and O_2 (K_{CO}/K_{O_2}), of Mb to the protoheme. The K_{CO}/K_{O_2} is about 20 000 for free protoheme, whereas that for sperm whale Mb is only 25 [25]. Therefore, while the inherent relative affinity of the ferrous heme for O_2 is lower than that for CO, the protein chain of Mb clearly alters the binding characteristics of the heme, dramatically increasing the O_2 affinity relative to that for CO. Along a long term investigation from X-ray crystallography, spectroscopy, and protein kinetics of native Mb and a series Mb mutants, the major factor that regulates such ligands discrimination and recognition in the heme pocket site is postulated as steric hindrance within the heme pocket and electrostatic interactions between the bound ligand and distal histidine [29].

The crystallography studies of CO bound heme compound suggest a linear Fe-C-O geometry in an orientation almost perpendicular to the heme plane [30,31]. Distortion from the linear Fe-C-O geometry was found in a series of studies on "picket fence" and "pocket" porphyrins [32-34]. In the latter compound, the additional steric hindrance near the ligand

binding site resulted in unaltered O_2 affinity but decreased CO affinity [32,33]. The early reported x-ray and neutron crystal structures of CO-bound Mb (MbCO) show bent binding geometries with substantial deviations from linearity. These studies led to the proposal of a steric hindrance arising from the highly conserved distal pocket residues such as Val (E11), Leu (B10), Phe (CD1) and His (E7) destabilizes the binding of CO. However, the latest results from high resolution crystal structure argue a nearly linear geometry as the most likely conformation of Fe-C-O in MbCO [4]. Instead of the bending of CO ligand, the two helices that hold the heme in place, helices E and F move slightly away from one another giving rise to the longer Val (E11) to CO distances observed in the MbCO structures. While O_2 binds at an angle to the heme normal, a smaller distortion of the polypeptide would be required to accommodate it [35,36]; hence the steric barrier for O_2 binding should be lower. These studies provide insight into ligand discriminations in MbCO regarding the mechanism of the steric hindrance from the residues located in distal pocket.

However, many studies of the mutant Mbs from spectroscopy and protein kinetics suggest that the major contribution to this discrimination results from electrostatic interaction between the bound O_2 and the distal His64 (Fig.1.4) [25,29]. In the unligated Mb, a water molecule is hydrogen bonded to the distal histidine and must be displaced in order for gaseous ligands to bind. This hydrogen bond brings an inhibition for all ligands binding by a factor of ~10. In the case of O_2 binding, the forming of strong hydrogen bond between His64 and highly polar FeO_2 complex stabilizes the O_2 by a factor of ~1000. The resulting net stabilization for bound O_2 is ~100 as compared with the bare heme compound or the mutated Mbs with an apolar residue at position 64. With respect to bound CO and NO, the electrostatic interaction with the histidine is much weaker. Compared with the bare heme, the electrostatic interaction with His64 only raises the stabilization ~2-3 fold for the bound CO and ~10 fold for the bound NO. After taking into account the inhibition factor of ~10 from the bound water in deoxyMb,

the stabilization due to the electrostatic interaction with His64 decrease 5-fold for CO and no change for NO binding. Recently, it becomes more and more accepted that stabilization of bound O_2 by the electrostatic interaction of His64 is much larger than by the direct steric hindrance of the distal residues.

1.1.4. Heme enzymes

Heme-enzymes are the early discovered kind of heme proteins that play an essential role in oxidative metabolism and electron transport system, such as peroxidases, catalase and peroxygenase P450 [37-39]. Heme is a good reservoir to the pool electrons or positive holes, and thus provides the redox potential required for a variety of catalytic reactions (oxidation, peroxidation, oxygenation and peroxygenation)

Peroxidases are found widespread in nature and are expressed by both prokaryotic and eukaryotic cells. Heme peroxidase appears to be significant covalent and structural variation is seen from mammals and plants, which catalyzes the one-electron oxidation of a variety of compounds by utilizing hydrogen peroxide [40]. The resting peroxidase reacts with hydrogen peroxide as an oxidant to yield an intermediate called compound I, which is reduced to the resting state via the second intermediate, compound II, by the use of reducing substrates. Catalase occurs in nearly all aerobic organisms, where its apparent function is to removal of small peroxides, particularly hydrogen peroxide, before they can cause cellular damage either directly or through their reactive breakdown products such as the highly reactive oxidant, the hydroxyl radical [41]. The overall reaction catalyzed by catalase is shown as $2H_2O_2 \rightarrow O_2+2H_2O$. Cytochromes P450 are a superfamily of heme-thiolate enzymes that mainly catalyze the monooxygenation of a wide array of apolar substrates [42]. This is a two-electron oxidation of substrate with one of the dioxygen-derived O atoms inserted into the C-H bond of substrate. Cytochromes P450 are isolated from all living organisms, including bacteria, fungi,

plants, insects, and vertebrates. P450s are involved in metabolizing a wide variety of hydrophobic compounds. The primary monooxygenation reaction catalyzed by a P450 is the following: $SH+O_2+NAD(P)H+H^+ \rightarrow SOH+NAD(P)^++H_2O$, where the SH and SOH denote substrate and product, respectively.

1.1.5. Heme-based sensor proteins

Heme-based sensor proteins are the recently discovered heme proteins, which play an important role in mediating transcriptional and regulatory events associated with the presence of gaseous diatomics, such as CO, NO and O_2 [43]. In a heme-based sensor, the regulatory heme-binding domain or subunit controls the neighboring transmitter region of the same protein. Such signal-transducing heme proteins govern adaptive responses to fluctuation in O_2, CO or NO: all three being diatomic gases that are now appreciated as physiological messengers. As a class of heme proteins, the sensors are distinct from the carriers of gases and the catalysts of oxygen-atom and electron transfer reactions. The transmitter regions of heme-based sensors typically feature modules that also transducer signals in many nonheme proteins; such modules include histidine protein kinase, cyclic-dinuchleotide phosphodiesterase, nucleotide cyclase, chemotaxis receptor, and DNA-binding transcription-factor activities [44-52]. The regulatory domains, on the other hand, have several architectural and sequence motifs that are entirely novel for heme binding, such as Per-Arnt-Sim (PAS), cyclic adenosine 3',5'-monophosphate (cAMP)-receptor-like, and modified-globin domains [53-55].

Soluble guanylate cyclase (sGC) acts as a physiological sensor for NO, which is the only discovered NO sensor among all the heme-based sensor proteins [56]. sGC is expressed in the cytoplasm of almost all mammalian cells, which catalyzes the conversion of 5'-guanosine triphosphate (GTP) to cyclic 3',5'-guanosine monophosphate (cGMP) in the presence of Mg^{2+} and Mn^{2+}. The mammalian sGC is a heterodimers, composing of two homologous subunits,

α and β and α_1 and β_1. However the sGC only contain one heme in the β_1–subunit, and His105 coordinates to the heme-iron in the proximal side [57,58]. N-terminal domain that binds the heme in the β_1-subunit is the sensor domain, and C-terminal domain that has the catalytic region. Upon NO binding to the heme in sGC, the conversion is increased up to 200-fold compared with its basal activity, whereas, binding of CO only increases the conversion about 5-fold.

The FixL proteins of *Rhizobia* are biological O_2 sensor, which regulate the nitrogen fixation gene expression by serving as the sensory of the FixL/FixJ two-component system [44,59]. FixLs contain a heme-sensor domain characterized as a PAS domain and a histidine kinase domain at C-terminal, which is regulated by the heme-PAS domain. The binding of O_2, the activity of kinase is repressed and kept in "off" state. The dissociation of O_2, the kinase undergoes autophosphorylation ("on" state), and transfer this phosphoryl group to its cognate response regulator, FixJ. Crystal structure of the heme-PAS domain reveals that a large shift in the F-G loop occurs during the transferring from "off" state to "on" state, and porphyrin plane become more flat from a ruffled structure [53].

E. coli direct oxygen sensor (*Ec* DOS) is a new class of heme-containing PAS protein, distinct from FixL. *Ec* DOS is composed of N-terminal PAS domain and C-terminal phosphodiesterase domain. Similar to the FixLs, *Ec* DOS appears as an O_2-sensor proteins. The phosphodiesterase domain is active in the deoxy state, but is inactive in O_2-bound or oxidized form [47].

Heme-based aeroxtaxis transducers (HemATs) are O_2 sensor heme proteins which consist of a sensor domain with myoglobin-like structure, and a Tsr-like cytoplasmic domain which mediates aerotaxis response. The discovery of HemATs suggests that the globin-like can function in regulation as well as ligand storage and transport [51].

CooA is a CO sensor because it responds to CO in a physiologically relevant range and induces expression of the genes required for *Rhodospirullum rubrum* to consume CO as a carbon source. CO binds to the ferrous 6-coordinate heme by displacing an endogenous protein ligand, this change in coordination induces binding of the functional domain to DNA and results in expression of the *coo* genes. The binding of CO regulate the DNA affinities and cause quite large conformational changes in the DNA-binding domain [49,54].

1.2. Aim of this Study

The iron protoporphyrin IX (*b* type heme) exists as a reaction center in most of the heme proteins as a prosthetic group which bound with the protein matrix. It carries out various functions including the diatomic gaseous ligand storage and transport, electron transfer, oxidization, peroxidization, catalysis and signaling process and so on. For investigating the active center, heme-iron-ligand complex, IR and visible RR spectroscopy have revealed the heme environment structure and the ligand discrimination mechanism for many heme proteins. Furthermore, electron paramagnetic resonance spectroscopy and quantum mechanism study have been used to revealing the reaction mechanism of heme enzyme. However, in any cases the accompanying conformational changes in protein moiety always occur for regulating protein function as revealed by x-ray crystallography. It appears quite important to establish a correlation between the active center, heme, and the protein matrix for understanding the essential mechanism for heme proteins. Also, this issue has attracted a lot of concerns from many fields. The nature utilizes *b* type heme as the most common structure among the four kinds of hemes that contain same framework but altered substitutions (Fig.1.3). Therefore, it is easy to propose that the side chains of heme could play important role in regulation of protein structure and function, and this propose is consistent with the discoveries from more and more

experimental data that side chains are involved in many reactions related with protein functions.

In this study we systematically investigate the role of propionate side chains of *b* type heme from structural and energetic viewpoint in Mb as a model molecule, because Mb is a monomer and has been study extensively from structure to function. As a well characterized protein, the findings in Mb along all the time were used as a paradigm for investigations of other heme proteins. The author hopes the investigations in this work could provide some underlying principles that are useful for other studies.

Reference:

1. Antonini, E., and Brunori, M. (1971) *Hemoglobin and myoglobin in their reactions with ligands.*, in Neuberger, A., and Tatum, E. L. Eds., *Frontiers in Biology*, **21**, North-Holland Publishing Company, Amsterdam
2. Kendrew, J. C., Dickerson, R. E., Strandberg, B. E., Hart, R. G., Davies, D. R., Phillips, D. C., and Shore, V. C. (1960) *Nature* **185**, 422
3. Perutz, M. F., Rossmann, M. G., Cullis, A. F., Muirhead, H., Will, G., and North, A. C. T. (1960) *Nature* **185**, 416
4. Kachalova, G. S., Popov, A. N., and Bartunik, H. D. (1999) *Science* **284**, 473
5. Kavanaugh, J. S., Rogers, P. H., Arnone, A., Hui, H. L., Wierzba, A., Deyoung, A., Kwiatkowski, L. D., Noble, R. W., Juszczak, L. J., Peterson, E. S., and Friedman, J. M. (2005) *Biochemistry* **44**, 3806
6. Kendrew, J. C., Bodo, G., Dintzis, H. M., Parrish, R. G., Wyckoff, H., and Phillips, D. C. (1958) *Nature* **181**, 662
7. Gibson, Q. H. (1959) *Biochem. J.* **71**, 198
8. Perutz, M. F. (1970) *Nature* **228**, 726
9. Perutz, M. F. (1972) *Nature* **237**, 495
10. Fischer, H., and Zeile, K. (1929) *Justus. Liebigs Ann. Chem.* **468**, 98
11. O'Brian, M. R., and Thony-Meyer, L. (2002) in *Advances in Microbial Physiology,* Academic Press, 257
12. Mogi, T., Saiki, K., and Anraku, Y. (1994) *Mol. Microbiol* **14**, 391
13. Brown, K. R., Allan, B. M., Do, P., and Hegg, E. L. (2002) *Biochemistry* **41**, 10906
14. Sano, S., and Tanaka, K. (1964) *J. Biol. Chem.* **239**, PC3109
15. Martinez, S. E., Huang, D., Ponomarev, M., Cramer, W. A., and Smith, J. L. (1996) *Protein Sci* **5**, 1081

16. Barker, P. D., Nerou, E. P., Cheesman, M. R., Thomson, A. J., de Oliveira, P., and Hill, H. A. O. (1996) *Biochemistry* **35**, 13618

17. Tomlinson, E. J., and Ferguson, S. J. (2000) *PNAS* **97**, 5156

18. Vainshtein, B. K., Melik-Adamyan, W. R., Barynin, V. V., Vagin, A. A., Grebenko, A. I., Borisov, V. V., Bartels, K. S., Fita, I., and Rossmann, M. G. (1986) *Journal of Molecular Biology* **188**, 49

19. Hargrove, M. S., Wilkinson, A. J., and Olson, J. S. (1996) *Biochemistry* **35**, 11300

20. Breslow, E., and Koehler, R. (1965) *J. Biol. Chem.* **240**, 2266

21. Fermi, G., and Perutz, M. F. (1981) in *Haemoglobin and Myoglobin. Atlas of Biological Structures* (Phillips, D. C., and Richards, F. M.ed), Clarendon, Oxford

22. Dickerson, R. E., and Geis, I. (1983) in *I. Hemoglobin* Benjamin Cummings, Menlo Park, CA

23. Chan, M. K. (2001) *Curr. Opin. Chem. Biol.* **5**, 216

24. Brantley Jr, R. E., Smerdon, S. J., Wilkinson, A. J., Singleton, E. W., and Olson, J. S. (1993) *J. Biol. Chem.* **268**, 6995

25. Olson, J. S., and Phillips Jr, G. N. (1997) *J. Biol. Inorg. Chem.* **2**, 544

26. Traylor, T. G., Mitchell, M. J., Tsuchiya, S., Campbell, D. H., Stynes, D. V., and Koga, N. (1981) *J. Am. Chem. Soc.* **103**, 5234

27. Traylor, T. G., White, D. K., Campbell, D. H., and Berzinis, A. P. (1981) *J. Am. Chem. Soc.* **103**, 4932

28. Olson, J. S., McKinnie, R. E., Mims, M. P., and White, D. K. (1983) *J. Am. Chem. Soc.* **105**, 1522

29. Springer, B. A., Sligar, S. G., Olson, J. S., and Phillips Jr, G. N. (1994) *Chemical Reviews* **94**, 699

30. Peng, S.-M., and Ibers, J. A. (1976) *J. Am. Chem. Soc.* **98**, 8032

31. Ray, G. B., Li, X. Y., Ibers, J. A., Sessler, J. L., and Spiro, T. G. (1994) *J. Am. Chem. Soc.* **116**, 162

32. Collman, J. P., Brauman, J. I., Halbert, T. R., and Suslick, K. S. (1976) *PNAS* **73**, 3333

33. Collman, J. P., Brauman, J. I., Iverson, B. L., Sessler, J. L., Morris, R. M., and Gibson, Q. H. (1983) *J. Am. Chem. Soc.* **105**, 3052

34. Gerothanassis, I. P., Momenteau, M., Hawkes, G. E., and Barrie, P. J. (1993) *J. Am. Chem. Soc.* **115**, 9796

35. Slebodnick, C., and Ibers, J. A. (1997) *J. Biol. Inorg. Chem.* **2**, 521

36. Vojtechovsky, J., Chu, K., Berendzen, J., Sweet, R. M., and Schlichting, I. (1999) *Biophys. J.* **77**, 2153

37. Denisov, I. G., Makris, T. M., Sligar, S. G., and Schlichting, I. (2005) *Chem. Rev.* **105**, 2253

38. Dawson, J. H. (1988) *Science* **240**, 433

39. Isaac, I. S., and Dawson, J. H. (1999) *Essays Biochem.* **34**, 51

40. Jones, P. (2001) *J. Biol. Chem.* **276**, 13791

41. Zamocky, M., and Koller, F. (1999) *Progress in Biophysics and Molecular Biology* **72**, 19

42. Montellano, R. O. (1986) *Cytochrome P-450 Structure, Mechanism and Biochemistry*, in Montellano, R. O. Eds., Plenum Press, New York and London, 217

43. Rodgers, K. R. (1999) *Curr. Opin. Chem. Biol.* **3**, 158

44. Gilles-Gonzalez, M. A., Gonzalez, G., and Perutz, M. F. (1994) *Biochemistry* **33**, 8067

45. Craven, P. A., and DeRubertis, F. R. (1978) *J. Biol. Chem.* **253**, 8433

46. Gilles-Gonzalez, M. A., Ditta, G. S., and Helinski, D. R. (1991) *Nature* **350**, 170

47. Delgado-Nixon, V. M., Gonzalez, G., and Gilles-Gonzalez, M. A. (2000) *Biochemistry* **39**, 2685

48. Chang, A. L., Tuckerman, J. R., Gonzalez, G., Mayer, R., Weinhouse, H., Volman, G., Amikam, D., Benziman, M., and Gilles-Gonzalez, M. A. (2001) *Biochemistry* **40**, 3420

49. Shelver, D., Kerby, R. L., He, Y., and Roberts, G. P. (1997) *Proc. Natl. Acad. Sci. U. S. A.* **94**, 11216

50. Dioum, E. M., Rutter, J., Tuckerman, J. R., Gonzalez, G., Gilles-Gonzalez, M. A., and McKnight, S. L. (2002) *Science* **298**, 2385

51. Hou, S., Larsen, R. W., Boudko, D., Riley, C. W., Karatan, E., Zimmer, M., Ordal, G. W., and Alam, M. (2000) *Nature* **403**, 540

52. Hou, S., Freitas, T., Larsen, R. W., Piatibratov, M., Sivozhelezov, V., Yamamoto, A., Meleshkevitch, E. A., Zimmer, M., Ordal, G. W., and Alam, M. (2001) *Proc. Natl. Acad. Sci. U. S. A.* **98**, 9353

53. Gong, W., Hao, B., Mansy, S. S., Gonzalez, G., Gilles-Gonzalez, M. A., and Chan, M. K. (1998) *Proc. Natl. Acad. Sci. U. S. A.* **95**, 15177

54. Lanzilotta, W. N., Schuller, D. J., Thorsteinsson, M. V., Kerby, R. L., Roberts, G. P., and Poulos, T. L. (2000) *Nature Structural Biology* **7**, 876

55. Zhang, W., and Phillips Jr, G. N. (2003) *Structure* **11**, 1097

56. Friebe, A., and Koesling, D. (2003) *Circ. Res.* **93**, 96

57. Wedel, B., Humbert, P., Harteneck, C., Foerster, J., Malkewitz, J., Bo?hme, E., Schultz, G., and Koesling, D. (1994) *Proc. Natl. Acad. Sci. U. S. A.* **91**, 2592

58. Zhao, Y., Schelvis, J. P. M., Babcock, G. T., and Marletta, M. A. (1998) *Biochemistry* **37**, 4502

59. Gilles-Gonzalez, M. A., and Gonzalez, G. (1993) *J. Biol. Chem.* **268**, 16293

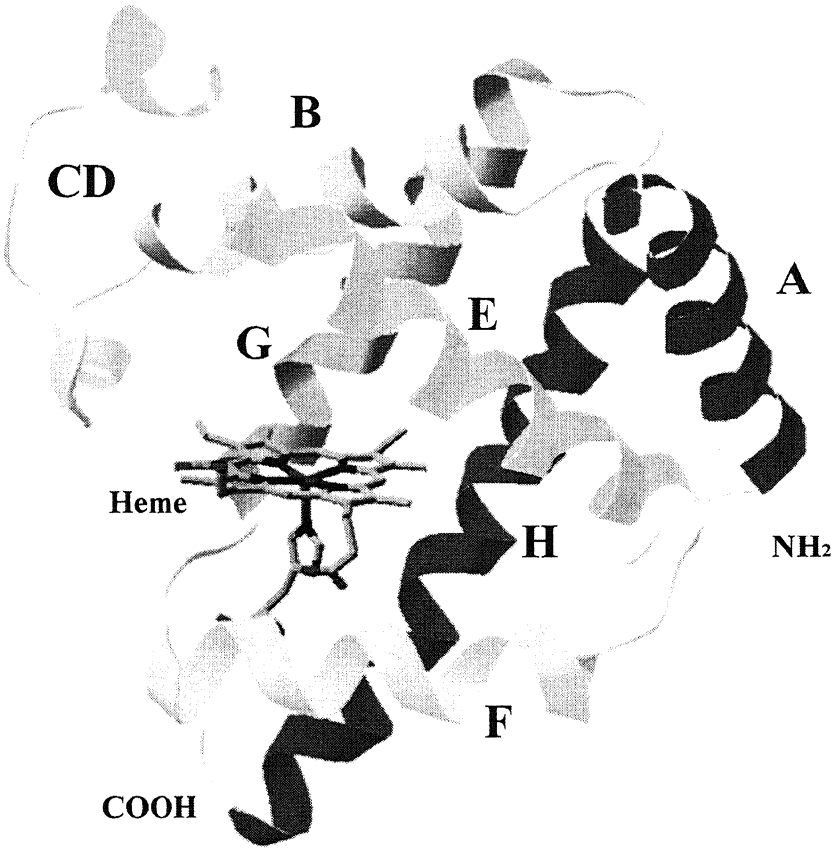

Fig.1.1. Crystal structure of deoxy form swMb (PDB code: 1BZP), helices are labeled from A to H (taken from ref. 4).

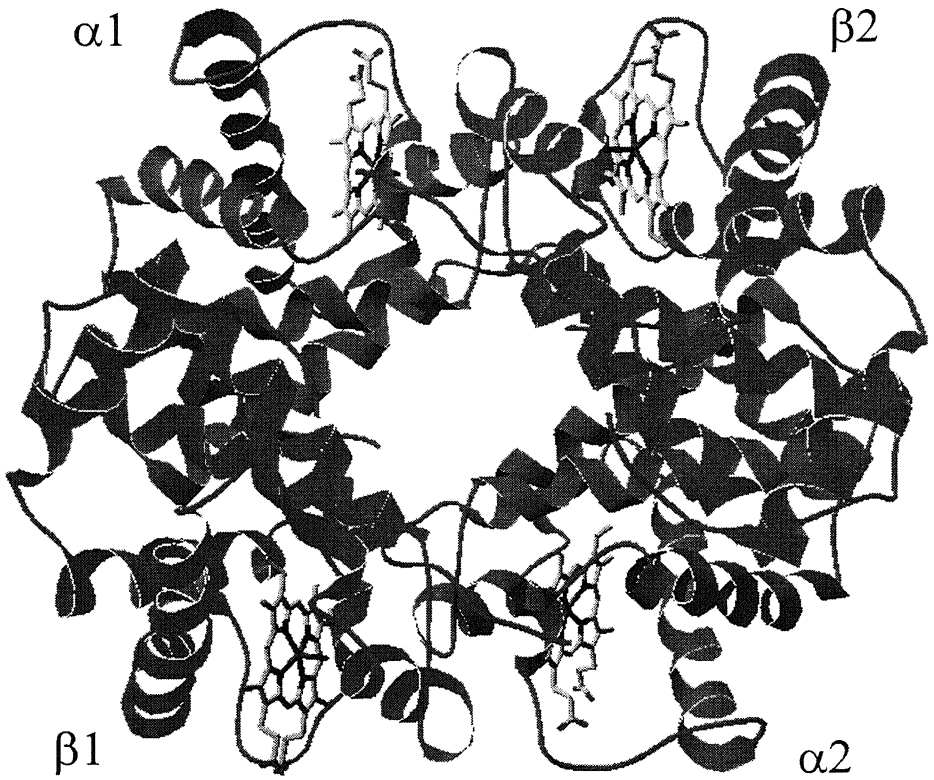

Fig.1.2. Crystal structure of deoxy form Hb (PDB code: 1XZ2), heterodimers labeled by α1β1 and α2β2 (taken from ref. 5).

A

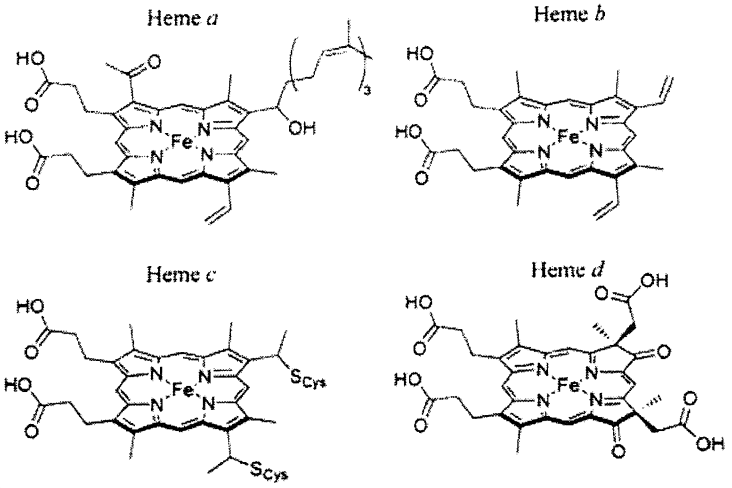

B

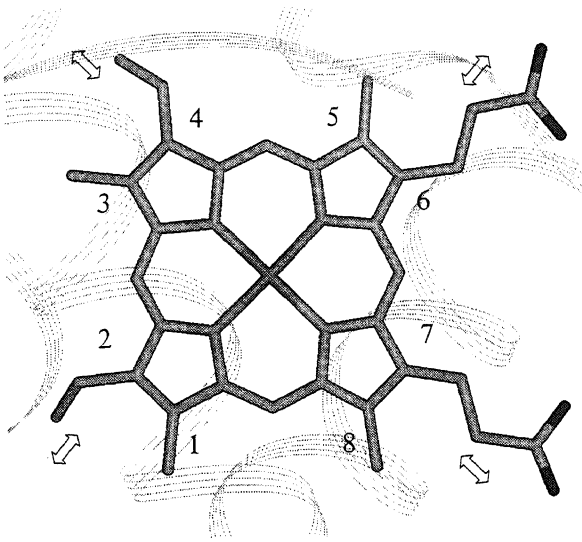

Fig.1.3. Panel A shows structures of heme *a-d*, panel B shows the structure of heme *b* with labeled substitutions, and arrows indicate the interaction with surrounding protein residues.

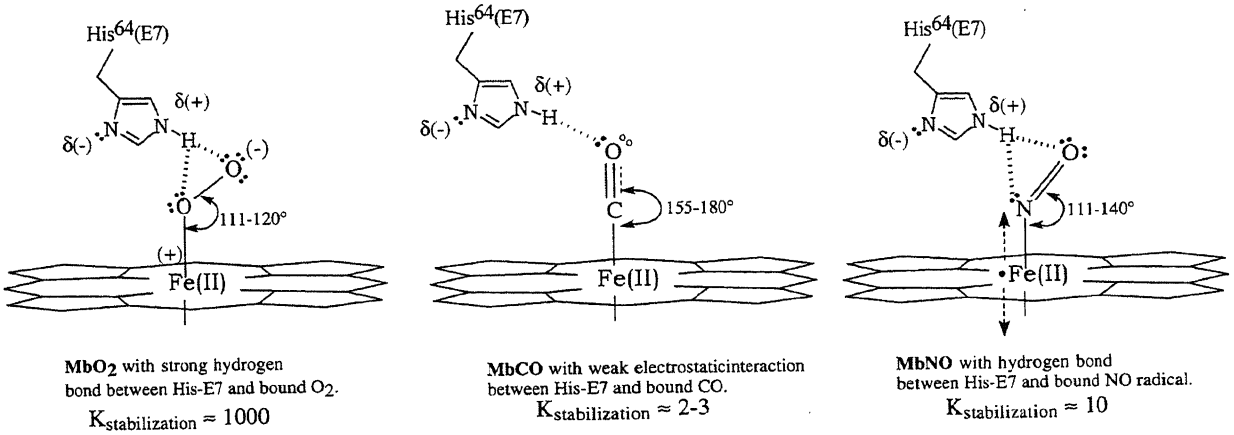

Fig.1.4. Proposed structures of ligand binding geometry and electrostatic interactions with distal histidine of O_2, CO and NO in native sperm whale myoglobin (taken from ref. 23).

Chapter 2. Pathway of Information Transmission in Myoglobin Revealed by UV Resonance Raman Spectroscopy

(J. Biol. Chem.2006, 281, 24637-24646)

2.1. Overview

2.1.1. Signal transduction in heme sensor protein

Hb provides the most classical example for understanding of heme-signaling to the surrounding protein environment [1]. The O_2 binding signal is communicated to another heme through the subunit-subunit interface, resulting in an increase of oxygen affinity. This cooperativity reflects the heme-heme interactions which rely on protein higher order structural changes, triggered by the shift of the iron atom into the heme plane upon oxygen binding. In this section we briefly visit some heme sensor proteins from the viewpoint of the signaling mechanism.

The activation of sGC is proposed to results from the cleavage of the proximal covalent bond between the Fe and His105 upon NO binding to Fe [2,3]. Changes of heme structure from 6- to 5-coordinate results in a conformational change in protein that triggers the phosphate group transfer and cyclization producing cGMP from GTP. However, it was found that the binding of CO also can activate this enzyme as well as NO in the presence of the activator, 3-(5'-hydroxymethly-2'-furyl)-1-benzylindazole (YC-1) [4]. This observation indicates that there might be another triggering mechanism in the case of CO with YC-1, different from that in NO case, because the 6-coordinate heme exists in CO-bound/YC-1 sGC [5]. It was proposed that the binding of CO in presence of YC-1 induces structural change of the heme-vinyl as well as propionate groups that adopt a specific conformation [6,7]. This conformation must be responsible for the activation of sGC. Therefore a proximal or heme peripheral pathway could play important roles in signaling of sGC.

FixLs and *Ec* DOS belong to the heme-PAS protein family [8,9]. The current x-ray crystal data reveals that the alternative hydrogen-bonding interactions between the ligand-free and ligand-bound state plays a central role for stimulating the activity of enzyme. As for *Bj*FixLH, the binding of O_2 forces Arg220 to rupture its salt bridge to the 7-propionate in the unligated

(ferric/deoxy) state and then to move to the distal heme pocket and to form a hydrogen bond with O_2. Subsequently, Arg206 forms a hydrogen bond with the released 7-propionate. In contrast, the binding of NO and CO does not cause such an alteration in salt bridges [10]. Distinct from FixLs, the binding of gaseous ligand to *Ec* DOS causes the displacement of an endogenous axial ligand, Met95. Specifically, a hydrogen bond between the 7-propionate and Met95 is replaced by a hydrogen-bonding network between 7-propionate, Arg97, and heme-coordinated O_2 upon O_2 binding [11,12]. This significant structure rearrangement between heme side chains and surrounding peptide suggests a large conformational change in the sensor PAS domain is required for signal transduction and regulation of the functional domain.

2.1.2. Ultraviolet Resonance Raman Spectroscopy (UVRR)

Raman and IR spectroscopy are the useful tool to detect the vibrational information of molecules and they usually provide the complementary information about molecular structures. In the biologic organism, most of proteins exist in aqueous environments. In order to establish the real relationship between the structure and function, the best way is monitoring proteins in solution which is close to their natural environments. In respect of this viewpoint, Raman spectroscopy has advantages in monitoring subtle structural changes for proteins, because the Raman scattering from water is quite weak and negligible when compared with IR spectroscopy. Another advantage is the selective enhancement that is possible in certain kinds of vibrations of a chromophoric group in a molecule when the incident light is chosen for the corresponding absorption maximum of electronic transition. This is called resonance Raman effect (RR). Therefore, by using RR, the most clear and fine information can be obtained by the cost of minimum mount of protein samples. In the visible region, the RR is extensively applied to the chromophoric proteins, like heme proteins, flavoproteins, nonheme iron proteins

and some other metal-containing proteins. On the other hand, in the UV region, RR selectively provides the vibrations of the aromatic side chains and the polypeptide skeleton, which provide information about protein higher order structures and environments.

Tyr, Trp and Phe are the three aromatic amino acids among 20 kinds of amino acids. Trp has the most complicated structure compared with the others and the lowest distribution in proteins. Expect for Phe residue which has an apolar side chain, side chains of Tyr and Trp are polar and can form hydrogen bonds with other residues. Since the abundance of Phe residues exists in protein, people usually use Tyr and Trp rather than Phe as structural markers in protein matrix to gain more insight information. The Fig.2.1.1 shows the UVRR spectra of model compounds for L-tyrosine at pH 7.0 and 13.0 solution and L-tryptophan at pH7.0 solution excited at 229 nm. The Raman band of $NaClO_4$ at 933 cm^{-1} is used as an internal intensity standard for normalization. The bands arise from Tyr are labeled by Y, and those from Trp are labeled by W, followed by mode numbers according to the assignment given by Takeuchi and Harada [13]. Some of vibrational modes are illustrated in Fig.2.1.2.

The spectra-structure correlations have been established and used for interpretation of the protein UVRR spectra. This gives us some benefit, because various solvent effects for model compounds of Trp and Tyr that have known structures have been well investigated [14-17]. Both the wavenumber and intensity of a Raman band reflect the structure and interaction of vibrating atomic group that is responsible for the Raman band. For Trp vibrations (Fig.2.1.1a), W17 band (878 cm^{-1}) is a mixed mode of benzene vibration and pyrrole ring with a large displacement of N_1H motion along the direction of the N_1—H bond, and its wavenumber is sensitive to hydrogen bonding of indole ring. The relationship between vibrational modes of W17 and N_1—H stretching is shown as Fig.2.1.4 [18,19]. The higher frequency of W17 mode indicates stronger hydrogen bond. The middle frequencies at ~878 cm^{-1} as in Fig.2.1.1 and 2.1.3 mean the N_1H group involved in hydrogen bond with water molecules. W7 mode

(1362/1342 cm^{-1}) arises from the N_1C_8 stretching mode in the indole ring. The doublet originates from Fermi resonance in which this mode and the combination bands of out-of-plane bending vibrations [14]. The intensity ratio of this doublet (I_{1360}/I_{1340}) reflects the environmental hydrophobicity around Trp residue: the stronger the hydrophobicity the higher intensity ratio [14,15]. W3 mode arises from the C_2C_3 stretching mode in the pyrrole ring [18]. The corresponding band is observed at 1554 cm^{-1} in Fig.2.1.1a. The frequency of C_2C_3 stretching is affected by the torsion angle about C_2-C_3-C_β-C_α ($|\chi^{2,1}|$) [20]. From the systematic analysis of seven Trp derivatives in known structures has established the correlation of frequencies of W3 mode and the torsion angles $|\chi^{2,1}|$, which is represented as Fig.2.1.5 [18,20-22].

In tyrosine (Fig.2.1.1b), the Y1 mode is perturbed by a Fermi resonance interaction coupled with the overtone of an out-of-plane ring bending vibration, 2Y16a. The intensity ratio I_{850}/I_{830} is sensitive to the state of hydrogen bonding and ionization of tyrosine phenolic OH group [23]. Also it is observed that the intensity ratio is varied with the excitation wavelength, about 1:1 at 240 nm and above 2:1 at 200 nm for tyrosine in aqueous solution [24]. Y7a' (1260 cm^{-1}) is also sensitive for hydrogen bonding, but it usually appears as a weak band and overlapped with the amide III band of a protein [16,25].

The OH group of tyrosine is deprotonated when pH value is above 11 (spectrum c in Fig.2.1.1 and 2.1.3). Since tyrosyl electronic transitions are red shifted to 240 nm and more intense relative to tyrosine, the Raman signal is highly enhanced at 244 nm excitation [26], as we can see in Fig.2.1.3c. Accordingly, Y8a and Y9a are largely enhanced and significantly downshifted, while Y7a is not shifted but is slightly enhanced [24,26]. Those bands are used as good markers for proton transfer in proteins.

In this chapter, we applied UVRR spectroscopy to a series of myoglobins as models for heme-sensor proteins. The UVRR spectroscopy provided abundance of information regarding

a subtle change that occurs in proteins. It is demonstrated that UVRR is an excellent tool for protein conformational studies.

Reference:

1. Perutz, M. F., Wilkinson, A. J., Paoli, M., and Dodson, G. G. (1998) *Annu Rev Biophys Biomol Struct* **27**, 1
2. Lawson, D. M., Stevenson, C. E. M., Andrew, C. R., George, S. J., and Eady, R. R. (2003) *Biochem. Soc. Trans.* **31**, 553
3. Russwurm, M., and Koesling, D. (2004) *EMBO J.* **23**, 4443
4. Stone, J. R., and Marletta, M. A. (1998) *Chemistry and Biology* **5**, 255
5. Makino, R., Obayashi, E., Homma, N., Shiro, Y., and Hori, H. (2003) *J. Biol. Chem.* **278**, 11130
6. Pal, B., and Kitagawa, T. (2005) *J. Inorg. Biochem.* **99**, 267
7. Pellicena, P., Karow, D. S., Boon, E. M., Marletta, M. A., and Kuriyan, J. (2004) *Proc. Natl. Acad. Sci. U. S. A.* **101**, 12854
8. Gilles-Gonzalez, M. A., Ditta, G. S., and Helinski, D. R. (1991) *Nature* **350**, 170
9. Sasakura, Y., Hirata, S., Sugiyama, S., Suzuki, S., Taguchi, S., Watanabe, M., Matsui, T., Sagami, I., and Shimizu, T. (2002) *J. Biol. Chem.* **277**, 23821
10. Gong, W., Hao, B., and Chan, M. K. (2000) *Biochemistry* **39**, 3955
11. Park, H., Suquet, C., Satterlee, J. D., and Kang, C. (2004) *Biochemistry* **43**, 2738
12. Kurokawa, H., Lee, D. S., Watanabe, M., Sagami, I., Mikami, B., Raman, C. S., and Shimizu, T. (2004) *J. Biol. Chem.* **279**, 20186
13. Harada, I., and Takeuchi, H. (1986), in Clark, R. J. H., and Hester, R. E. Eds., *In Spectroscopy of Biological Systems, Advances in Spectroscopy*, **13**, John Wiley & Sons, New York, 113

14. Harada, I., Miura, T., and Takeuchi, H. (1986) *Spectrochim. Acta* **42 A**, 307

15. Miura, T., Takeuchi, H., and Harada, I. (1988) *Biochemistry* **27**, 88

16. Takeuchi, H., Watanabe, N., Satoh, Y., and Harada, I. (1989) *J. Raman Spectrosc.* **20**, 233

17. Hildebrandt, P. G., Copeland, R. A., Spiro, T. G., Otlewski, J., Laskowski Jr, M., and Prendergast, F. G. (1988) *Biochemistry* **27**, 5426

18. Takeuchi, H., and Harada, I. (1986) *Spectrochim. Acta* **42 A**, 1069

19. Takeuchi, H. (2003) *Biopolymers - Biospectroscopy Section* **72**, 305

20. Miura, T., Takeuchi, H., and Harada, I. (1989) *J. Raman Spectrosc.* **20**, 667

21. Maruyama, T., and Takeuchi, H. (1995) *J. Raman Spectrosc.* **26**, 319

22. Maruyama, T., and Takeuchi, H. (1997) *Biochemistry* **36**, 10993

23. Siamwiza, M. N., Lord, R. C., and Chen, M. C. (1975) *Biochemistry* **14**, 4870

24. Rava, R. P., and Spiro, T. G. (1985) *J. Phys. Chem.* **89**, 1856

25. Takeuchi, H., Harada, I., and Yoshida, H. (1991) *Biochimica et Biophysica Acta - Protein Structure and Molecular Enzymology* **1078**, 307

26. Asher, S. A., Ludwig, M., and Johnson, C. R. (1986) *J. Am. Chem. Soc.* **108**, 3186

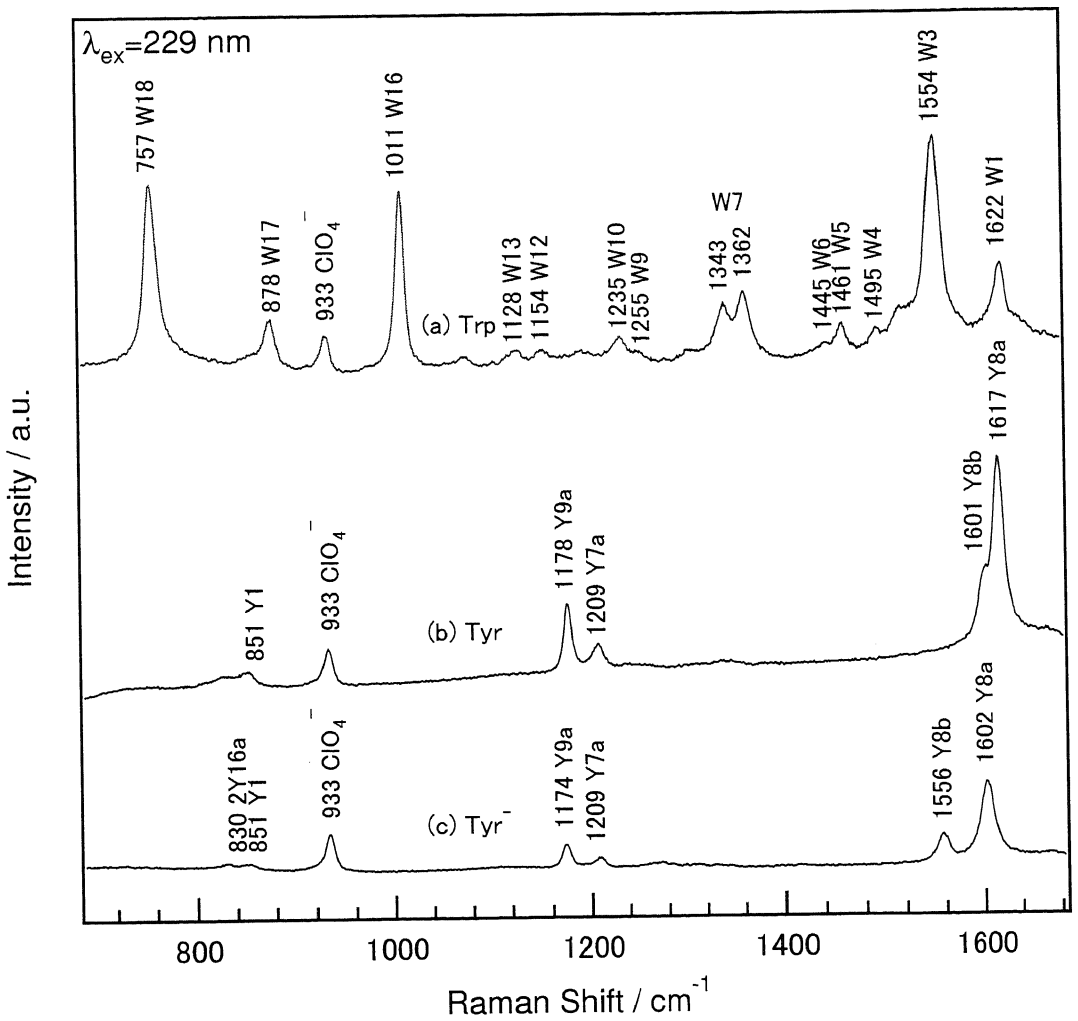

Fig.2.1.1. UVRR spectra of model compound at excitation wavelength of 229 nm. (a) L-Tryptophan and (b) L-Tyrosine at solution of pH 7.0 and (c) L-Tyrosine at solution of pH 13.0.

Tryptophan

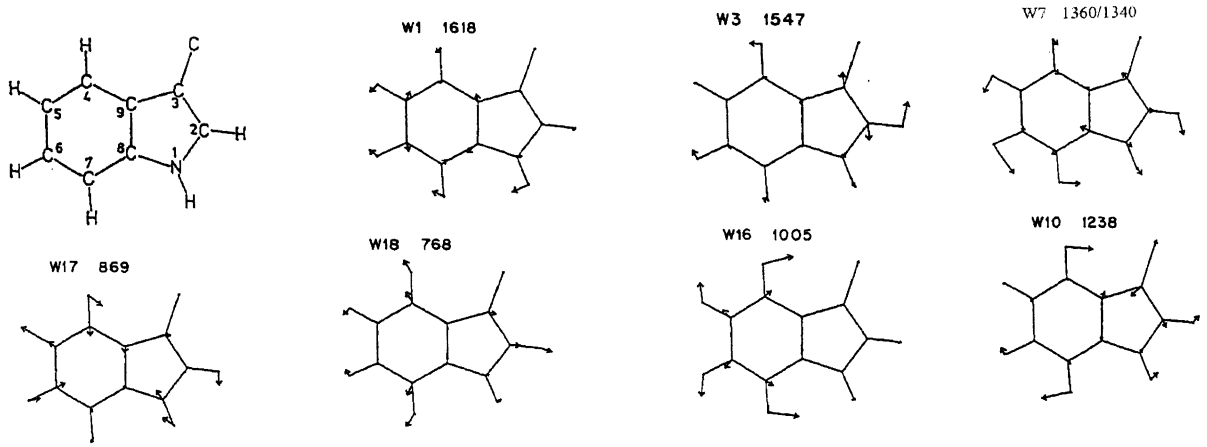

Tyrosine

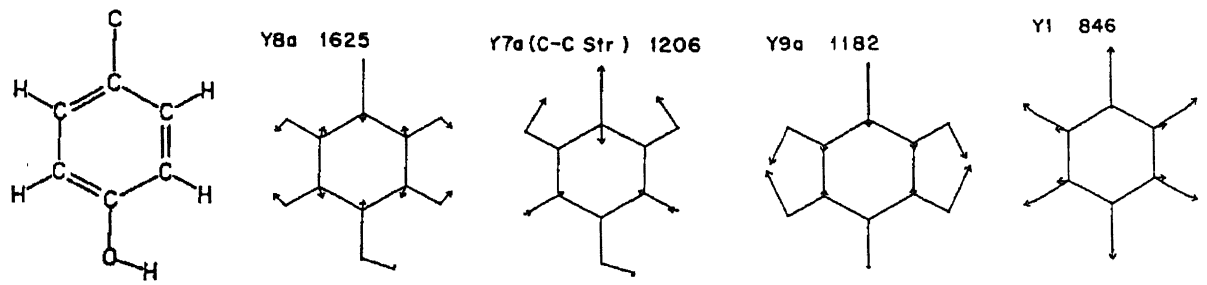

Fig.2.1.2. Atomic displacement vectors of some vibrational modes of 3-methyl indole (taken from ref. 13).

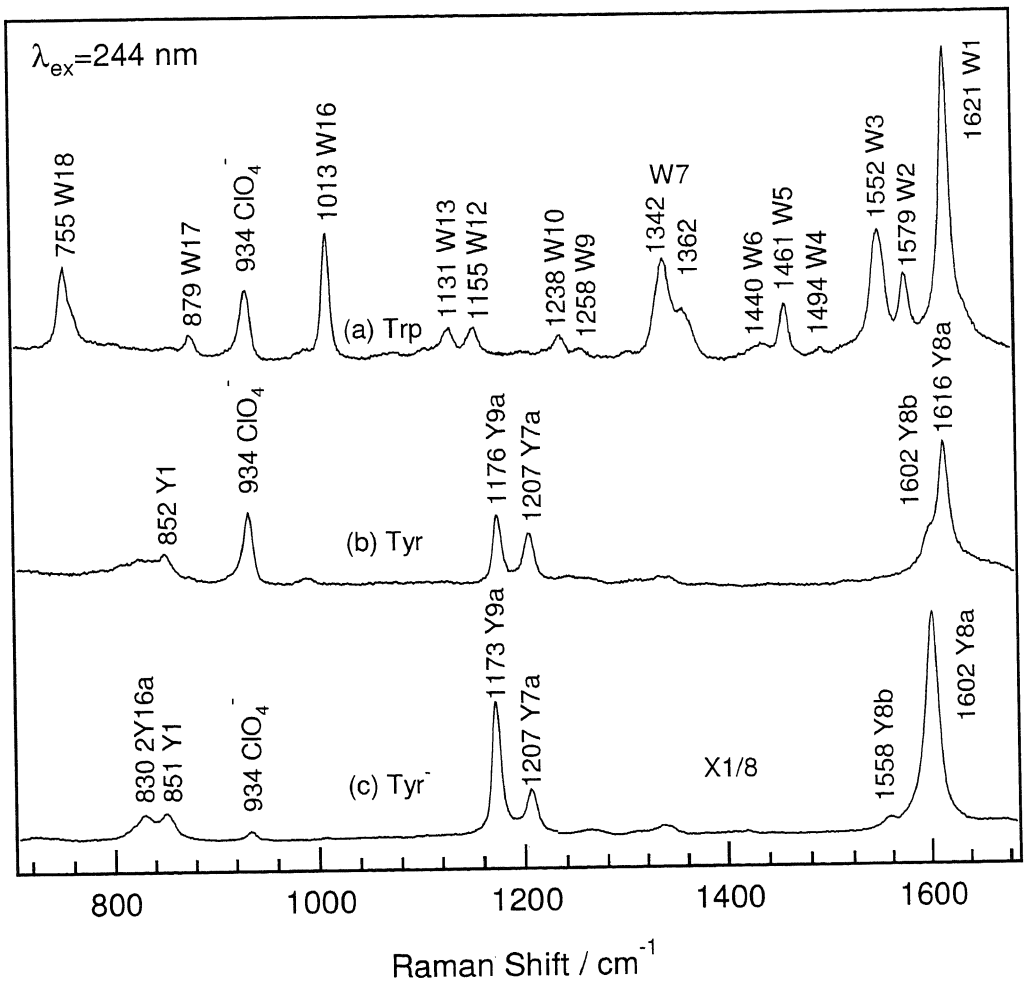

Fig.2.1.3. UVRR spectra of model compound at excitation wavelength of 244 nm. (a) L-Tryptophan and (b) L-Tyrosine at solution of pH 7.0 and (c) L-Tyrosine at solution of pH 13.0.

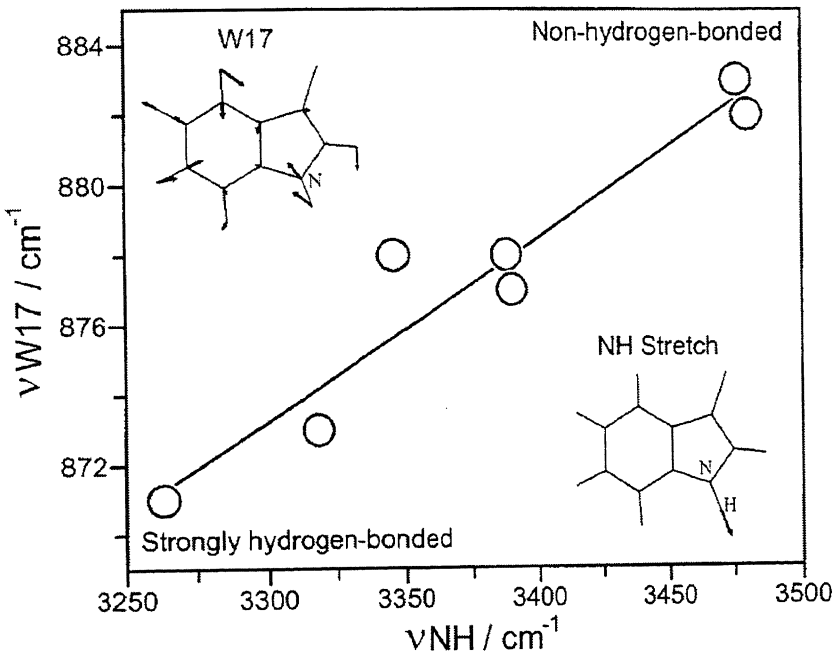

Fig.2.1.4. The linear relationship between the wavenumbers of W17 and the N-H stretch modes (taken from refs 18).

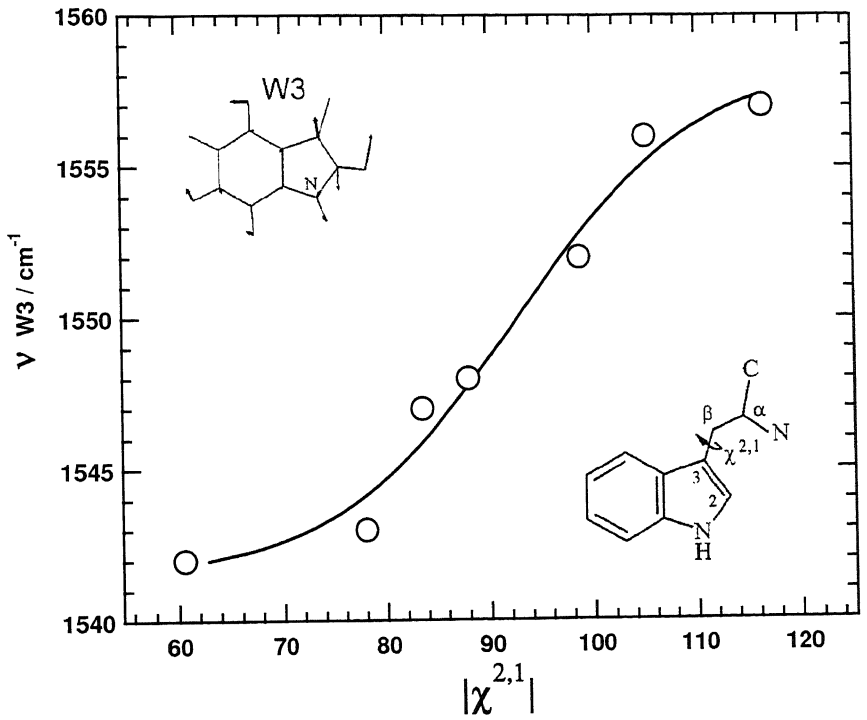

Fig.2.1.5. Wavenumbers of W3 plotted as a function of the absolute values of the torsional angle $|\chi^{2,1}|$ (taken from refs.18,20-22).

2.2. Pathway of Information Transmission from Heme to Protein upon Ligand Binding/Dissociation in Myoglobin Revealed by UV Resonance Raman Spectroscopy

2.2.1. Abstract

Gas sensory heme proteins respond to their environment by binding a specific gas molecule to heme and transmitting this primary binding signal to the protein. How the binding signal is transmitted from the heme to the protein remains to be clarified. Using UV resonance Raman (UVRR) spectroscopy, we investigated this pathway in sperm whale myoglobin as a model gas sensory heme protein. Based on the UVRR data and the effects of deleting one of three important pathways (His93, 6-propionate, or 7-propionate), we determined the changes in the conformation of globin that occur upon binding of CO, NO, or O_2 to heme and how they are transmitted from heme to globin. The UVRR results show that heme discriminates different ligands, resulting in different conformations in the globin protein. Specifically, NO induces changes in the spectrum of Trp residues in the A-helix that are significantly different from those induced by O_2 or CO binding. On the other hand, binding of O_2 to heme produces changes in the Tyr residues of the H-helix that are different from those induced by CO or NO binding. Furthermore, we found that cleavage of the Fe-His93 covalent bond eliminates communication to the terminal region of the H-helix and that the 7-propionate hydrogen-bonding network is essential for transmitting the CO or NO binding signal to the N- and C-termini. Finally, the 6-propionate is important only for NO binding. Thus, the hydrogen-bonding network in the protein appears to be critical for intramolecular signal transduction in gas sensory heme proteins.

2.2.2. Introduction

The structural change in heme that occurs upon ligand binding/dissociation is the main process underlying the cooperativity in oxygen binding by Hb [1] and signal transduction by gas sensory heme proteins [2-4]. This process is thought to mediate transmission of the heme ligand binding signal to the heme-binding domain of the protein. Mb is a small heme-containing protein that can reversibly bind diatomic gaseous molecules (O_2, NO, and CO). Because Mb is well characterized, it is an ideal model for investigating the interactions between heme and protein moiety of gas sensory heme proteins. The deoxyMb adopts a five-coordinate high-spin structure with the iron atom 0.3 Å out of the heme plane, whereas the heme is planar in the ligated form [5-8]. The out-of-plane displacement of the iron atom is thought to be responsible for a conformational change between the deoxy and ligated forms of Mb.

Our previous ultraviolet resonance Raman (UVRR) experiments, wherein Mb was excited at 244 nm, suggested that slight structural changes in Trp7 and Tyr151 occur upon CO binding [9]. In addition, time-resolved resonance Raman (RR) measurements of the Fe-His stretching mode with visible laser pulses have demonstrated that, for Mb, the structural change takes place rapidly (time constant of ~120 ps) [10]. However, the transmission of the heme structural change to globin *via* His93 has become a matter of controversy, because a fast structural change has also been observed for the Gly93(+Imd) mutant, which lacks the Fe-His covalent bond [11].

Fig.2.2.1 illustrates the hydrogen bonding networks in the vicinity of heme in sperm whale Mb (*sw*Mb) as revealed by X-ray crystallography [6]. The proximal His (His93) forms hydrogen bonds with Ser92 and Leu89. The CO_2^- group of the propionate side-chain at position 7 forms hydrogen bonds with His97 and Ser92, while the CO_2^- group of the propionate side-chain at position 6 participates in a hydrogen bonding network with Arg45, H_2O, and

His64 (distal His). It is very likely that these hydrogen bonding systems transmit conformational changes in heme upon ligand binding to the globin protein.

We next examined *sw*Mb by UVRR spectroscopy to explore the role of hydrogen bonds in this communication process. We first analyzed the conformational changes in Mb upon binding of various gaseous ligands (CO, NO, and O_2). We found that heme discriminates between different ligands by inducing significantly different conformations in the A- and H-helices. Furthermore, we monitored the UVRR spectral changes of Trp and Tyr residues that occur upon CO and NO binding to versions of Mb in which the predicted pathways for transmission of conformational changes (His93, 6-propionate, or 7-propionate) were eliminated by mutation or chemical modification of the heme. We found that the 7-propionate hydrogen bonding network in the heme proximal site is essential for communicating the conformational changes to the N- and C-termini upon binding of CO or NO to heme, whereas the 6-propionate pathway is important only for the communication of NO binding. Furthermore, we found that cleavage of the Fe-His93 covalent bond eliminates the communication to the C-terminus.

2.2.3. Experimental Procedures

Sample Preparation – Native (NT) *sw*Mb (Biozyme) and horse Mb (*h*Mb, Sigma) were used without further purification. Mb mutants including W7F-, W14F-, H93G(+Imd), S92A, and R45L Mb were expressed and purified as described previously [12,13] with some modifications [9]. Chemically modified hemes in which the 7- (7M6P) or 6-propionate (6M7P) of protoporphyrin IX was replaced by a methyl group were synthesized as described elsewhere [14]. The Fe(III) complexes were reconstituted into the *sw*Mb apoprotein [15]. The Fe-CO and Fe-His stretching modes of these preparations observed with visible RR spectra were not

significantly different from those of the NT Mb, although the heme spectra in the lower frequency region were distinct from that of the NT protein (see section: Appendix).

For UVRR measurements, the concentration of protein was adjusted to 200 and 300 μM in 50 mM phosphate buffer (pH 7.0) for excitation at 229 and 244 nm, respectively. As an internal intensity standard for UVRR difference spectra, 400 and 100 mM Na_2SO_4 were included in the samples for excitation at 229 and 244 nm, respectively. The ferric form of NT *sw*Mb was directly used from the commercial product. DeoxyMb was prepared by adding a minimal amount of sodium dithionite solution (final concentration 1–2 mM) to the protein solution under a nitrogen atmosphere. The O_2-bound form was prepared by passing the dithionite-reduced Mb protein through a small Sephadex G25 column under aerobic conditions and then saturating the sample with oxygen by flushing it with pure oxygen gas in a sealed Raman cell. The CO or NO adducts of Mb were prepared by introducing pure CO or NO gas into the Raman cell with an airtight syringe through a rubber septum. The formation of six-coordinate ligand-bound forms was confirmed by examining the optical absorption spectra.

UV Resonance Raman Measurements – UV resonance Raman measurements were performed as previously described [16]. The UV probe light at 229 nm or 244 nm was generated by an intracavity frequency-doubled Ar ion laser (Coherent; Innova 300 FReD). The second harmonic in the laser output was separated from the fundamental with a Pellin-Broca prism and focused into a protein sample solution. An ~100-μL aliquot of the sample solution was placed into a spinning cell with a stirring function [16]. Light scattered at a right angle was collected with the objective lens of a UV microscope, dispersed with a 126-cm single monochromator (Spex 1269) equipped with a 3600 groove/mm holographic grating, and detected with an intensified charge-coupled detector (Princeton Instruments; model ICCD-1024MG-E/1). The laser power at the sample point was 0.2–0.3 mW, and the spectral resolutions were set at 6.9 and 7.8 cm^{-1} for 244 nm and 229 nm excitations, respectively. The

protein sample was replaced with fresh one every 5–10 minutes, and the total exposure time to obtain each spectrum was ~1 h. The integrity of the sample after exposure to UV laser light was confirmed by comparing the visible absorption spectra obtained before and after the UVRR measurements. If some spectral changes were found, the Raman spectrum was discarded. Raman shifts were calibrated with cyclohexane, trichloroethylene, 1,2-dichloroethane, and toluene.

2.2.4. Results

Changes in the 229-nm-excited UVRR Spectrum of Mb upon Binding of Different Ligands – Fig.2.2.2 shows the raw 229-nm-excited UVRR spectrum of the deoxy (a) form of NT *sw*Mb and the deoxy – ferric (b), deoxy – O_2 (c), deoxy – CO (d), and deoxy – NO (e) difference spectra for NT *sw*Mb. The raw spectrum of NT *sw*Mb is dominated by the bands arising from two Trp (Trp7 and Trp14) and three Tyr (Tyr103, Tyr146, and Tyr151) residues, which are labeled W and Y, respectively, followed by their mode numbers [17]. Because the protein concentrations are the same in all measurements performed at a given excitation wavelength, the intensities of the Raman features were comparable in all of the raw spectra. The difference spectra were calculated so that the band for SO_4^{2-} (981 cm^{-1}), which was present at the same level in all samples as an internal intensity standard, would be zero.

Difference spectrum b shows strong negative bands at 758 (W18), 877 (W17), 1011 (W16), 1359 (W7), 1558 (W3), and 1616 cm^{-1} (Y8a/W1), indicating an increase in the intensity of the Trp and Tyr bands in the ferric form. Because of the importance of the physiological ligand, O_2, for Mbs, we examined the UVRR spectral changes of NT Mb upon binding of O_2. It is known that in the O_2 bound form, the heme iron is rapidly photo-oxidized even at very low laser power. The absorption spectra showed that the sample was partially oxidized to the ferric form (~30%) after exposure to the UV light, independently of pH 7 to 9 of solution. Thus, to obtain

the spectrum of the O_2-bound form, we subtracted the contribution of the spectrum of the ferric form from the observed spectrum. The resulting UVRR spectral changes upon O_2 binding are displayed in spectrum c. The low signal-to-noise ratio of spectrum c is due to this double-difference procedure. The deoxy – O_2 spectrum (c) reveals small features near the W18, W16, and W3 bands, implying that the intensity of the Trp Raman bands are slightly enhanced in the O_2-bound form. Spectrum d displays negative features similar to those observed upon O_2 binding (c); however, the features at the W16 and W18 modes seem to be stronger in the CO-bound than the O_2-bound form (Fig.S2.2.1). In contrast, spectrum e (deoxy – NO) yields very strong positive peaks for almost all Trp bands, indicating a large decrease in intensity for the Trp bands in the NO-bound form. Thus, the UVRR difference spectra show that, upon NO binding, the Trp Raman bands undergo spectral changes that are the opposite of those that occur upon CO and O_2 binding.

Assignment of Trp Spectral Changes Induced by CO Binding in the 229-nm-excited Spectra – Fig.2.2.3 displays the raw UVRR spectrum of the deoxy form (a) of NT *sw*Mb excited at 229 nm and the deoxy – CO difference spectra for NT (b), W14F- (c), and W7F-Mb (d). The frequency of the W17 band (~875 cm^{-1}) serves as a marker of hydrogen bonding of the Trp indole ring [18]. This band of NT Mb (a) appears at 877 cm^{-1}, indicating moderate strength of hydrogen bonding, consistent with the crystal structure, wherein both Trp7 and Trp14 form hydrogen bonds with water molecules [6].

The W7 band appears as a doublet at 1360/1340 cm^{-1} in the raw spectrum of NT Mb (a). The expanded spectra W7 bands of the W7F- and W14F-Mb are displayed in inset A of Fig.2.2.3. This doublet arises from Fermi resonance between the N_1–C_8 stretching fundamental (W7 mode) and the combination of out-of-plane bending vibrations [17]. The intensity ratio of the W7 doublet serves as a marker of the hydrophobicity of the environment around the indole

ring [17,18]. The I_{1358}/I_{1340} ratio for Trp14 is larger than that for Trp7, which is consistent with the fact that Trp14 is buried in a more hydrophobic environment than Trp7 [5,6].

The frequency of the Trp W3 mode is sensitive to the absolute value of the torsion angle ($|\chi^{2,1}|$) about the bond (C_β-C_3) connecting the indole ring to the peptide main chain [18]. It appears at 1558 cm^{-1} in spectrum a, and expanded spectra for NT and the W14F- and W7F-Mb (inset B of Fig.2.2.3) indicate that the more precise frequencies are 1557 cm^{-1} for Trp7 and 1560 cm^{-1} for Trp14. The 1557 cm^{-1} band for Trp7 suggests a $\chi^{2,1}$ of 114°, which is comparable to the value of 118° determined from the crystal structure [6]; however, the frequency of 1560 cm^{-1} for Trp14 is unexpectedly high and does not fit well with the empirical correlation curve [18].

As shown in Fig.2.2.3b, the W18, W17, W16, W7, and W3 bands of NT Mb exhibit prominent negative features, implying an increase in intensity of the Trp bands in the CO-bound form. Similar features have been observed for the W14F-Mb (Fig.2.2.3c). The difference spectrum of W7F-Mb (Fig.2.2.3d), however, displays no such negative features. These results indicate that the spectral changes that occur in NT Mb upon CO binding mainly arise from Trp7 rather than from Trp14.

Changes in the 229-nm-excited UVRR Spectrum upon CO Binding to Mb with a Modified Heme and Mutant Mbs – Fig.2.2.4 shows the raw UVRR spectrum of NT deoxyMb (a) excited at 229 nm and the deoxy – CO difference spectra for NT (b), H93G(+Imd) (c), 6M7P- (d), 7M6P- (e), and S92A Mb (f). Unexpectedly, the difference spectrum for H93G(+Imd) (c), in which exogenous imidazole is bound as a ligand of iron instead of His93, is very similar to that of NT (b) despite the absence of a covalent bond between the heme and globin. Because this strongly suggests that the Fe-His93 bond is not directly responsible for the spectral change of Trp7, we examined other possibilities by obtaining spectra d–f. As described by Hayashi et al.

[14], we synthesized the modified iron-protoporphyrins in which the 6- or 7-propionate is selectively replaced by a methyl group and used them to reconstitute Mb apoprotein (6M7P- and 7M6P-Mb, respectively). The deoxy – CO difference UVRR spectra were obtained in a similar way as for NT Mb. The difference spectrum of 6M7P-Mb (d) exhibits negative features for Trp bands similar to those observed for NT Mb (b). In contrast, the difference spectrum of 7M6P-Mb (e) shows small positive/large negative peaks at 750/760 and 1006/1014 cm^{-1}. In addition, a strong negative peak appeared at 1562 cm^{-1} (W3) in contrast to the negative peak at 1557 cm^{-1} in spectra b–d (see inset of Fig.2.2.4). This frequency shift is probably caused by an upshift of the Trp7 W3 band coupled with a large increase in intensity upon CO binding and may indicate a slight increase (10°–20°) in the $\chi^{2,1}$ angle of Trp7 [9,18]; however, we cannot rule out the possibility that Trp14 undergoes spectral changes in 7M6P-Mb because W3 of Trp14 is located at 1560 cm^{-1}. Regardless, the spectrum of 7M6P-Mb (e) differs significantly from the spectra of NT and H93G(+Imd) Mb, indicating that the structural change in Trp7 was perturbed by removal of the 7-propionate group or its hydrogen bonding network.

To confirm the effect of hydrogen bonding by 7-propionate, its hydrogen-bonding partner, Ser92 (Fig.2.2.1) was replaced with Ala (Fig.2.2.4, spectrum f). Its spectrum is similar to spectrum e but different from spectrum b. Furthermore, the difference spectra (e and f) reveal a derivative pattern near 1616 cm^{-1}, indicating an upshift of the Y8a/W1 frequency in the CO-bound form, whereas this frequency is not up shifted in spectra b–d. Consequently, we concluded that the structural change of heme upon CO binding is communicated to Trp7 *via* the hydrogen-bonding network through the 7-propionate and Ser92.

Assignments of Spectral Changes upon NO Binding in the 229-nm-excited Spectra – Fig.2.2.5 displays the raw UVRR spectrum of the deoxy form of NT Mb (a) and the deoxy – NO difference spectra of NT (b), W14F- (c), and W7F-Mb (d), respectively. Spectrum b has

strong positive peaks at W18, W17, W16, W7, and W3 mode, indicating a large decrease in the intensity of Trp bands in the NO-bound form. Some weak positive features are observed in the spectrum for Trp7 (W14F-Mb; c), whereas the spectrum for Trp14 (W7F-Mb; d) has stronger positive features. More precisely, the doublet-like positive peak for W18 in spectrum b arises from the contributions of both Trp7 (c) and Trp14 (d), which have slightly different W18 frequencies and intensities (see inset of Fig.2.2.5). On the other hand, the W16, W7, and W3 bands in the spectrum for NT Mb (b) can be regarded as the summation of spectra c and d, that is, simple addition of the changes in Trp7 and Trp14. Thus, both Trp7 and Trp14 show spectral changes upon NO binding.

UVRR Spectral Changes of Mb Mutants upon NO Binding in the 229-nm-excited Spectra – Fig.2.2.6 shows the raw UVRR spectrum of the deoxy form of NT *sw*Mb (a) and the deoxy – NO difference spectra for NT (b), H93G(+Imd) (c), S92A (d), and R45L Mb (e). The spectra for H93G(+Imd) (c) and NT Mb (b) are the same and show positive bands at W18, W17, W16, W7, and W3 mode. In contrast, mainly negative features are observed in the difference spectra for S92A (d) and R45L Mb (e). The spectrum for S92A Mb (d), which is expected to reflect the contribution of hydrogen bonding through the 7-propionate, exhibits large negative/small positive peaks at 753/771 and 1007/1013 cm^{-1}, which are produced from frequency downshifts of W18 and W16 upon NO binding, respectively, and negative peaks at 1558 and 1616 cm^{-1}. On the other hand, R45L Mb, which is expected to reflect the contribution of hydrogen bonding through the 6-propionate, yields mainly negative peaks. Thus, the spectral changes observed upon NO binding for H93G(+Imd) and NT Mb are similar, whereas the spectral changes for both S92A and R45L Mb are distinct.

Changes in the 244-nm-excited UVRR Spectrum of Mb upon Binding of Different Ligands – The raw UVRR spectrum of the deoxy form of NT *sw*Mb is shown in trace a of Fig.2.2.7. The Tyr bands are significantly enhanced compared with Fig.2.2.2(a). Trace b shows the deoxy – CO difference spectrum of NT *sw*Mb, revealing a derivative pattern near 1177 cm^{-1} (Y9a), thus indicating an upshift of the Y9a frequency in the CO-bound form. This change was not observed for *h*Mb, which lacks Tyr151 (replaced by Phe), and therefore is attributed to Tyr151 in *sw*Mb [9]. The most prominent feature in spectrum b is a positive peak at 1619 cm^{-1}, which is due to a decrease in intensity of the Y8a band in the CO-bound form. It may also contain contributions from C=C stretching of heme vinyl groups. In addition, it shows a positive feature at 1560 cm^{-1}, indicating an increased intensity of W3 in the deoxy form. These changes in spectrum b are identical to those observed previously by Haruta *et al.* [9].

Traces c and d of Fig.2.2.7 show the difference spectra of the deoxy – NO forms of *sw*Mb and *h*Mb, respectively, and traces e and f show the difference spectra of deoxy – O_2 and deoxy – ferric forms of *sw*Mb, respectively. The intensity-normalized raw spectra of the Y9a band are displayed in the inset for the ligand-bound (dotted line) and -free forms (solid line) as references for the difference spectra shown in traces b–f. Trace c reveals a derivative feature at 1177 cm^{-1} and a positive band at 1619 cm^{-1}, similar to those observed upon CO binding.

To assign the spectral change of the Y9a band observed upon NO binding by *sw*Mb, we examined the UVRR spectra of *h*Mb, which lacks Tyr151. Trace d shows the deoxy – NO difference spectrum of NT *h*Mb, which has a small negative peak instead of a derivative. This indicates a small increase in intensity without a frequency shift for Tyr103 and Tyr146 upon NO binding. Accordingly, the upshift in Y9a upon NO binding in *sw*Mb can be attributed to Tyr151.

We additionally examined the UVRR spectral changes of NT Mb upon binding of O_2 and subtracted the ferric contribution to the O_2-bound form in a way similar to that carried out for

the 229-nm excitation (Fig.2.2.2c). The UVRR spectral changes upon O_2 binding, displayed in spectrum e, reveal a positive feature near Y9a, implying a decrease in intensity for the O_2-bound form. We noted that the reduction in intensity of Y9a upon O_2 binding is coupled with a frequency upshift (see Fig.2.2.7 inset). In addition, the Y8a band (1619 cm^{-1}) of the O_2-bound form (e) appears less intense than the positive peaks in spectra b and c. We further noted that trace f displays features at W3 and Y8a distinct from those observed upon O_2 binding. Therefore, we concluded that the spectral changes of Tyr caused by O_2 binding, especially those near the Y9a band (traces b–e), differ from those observed caused by NO and CO binding.

Changes in the 244-nm-excited UVRR Spectrum upon CO Binding to Mb with a Modified Heme and Mutant Mbs – Fig.2.2.8 shows the raw UVRR spectrum of the deoxy form of NT *sw*Mb excited at 244 nm and the deoxy – CO difference spectra of NT (b), H93G(+Imd) (c), 6M7P- (d), R45L (e), 7M6P- (f), and S92A Mb (g).

H93G(+Imd) (c) exhibits a negative Y9a peak, which appears to be different from other spectra. Arg45 is a hydrogen-bonding partner of 6-propionate (Fig.2.2.1), and, therefore, its mutation to Leu disrupts the hydrogen-bonding network through 6-propionate. The difference spectra for 6M7P- (d) and R45L Mb (e) are very similar and have features like those observed for NT Mb (b). On the contrary, the features at 1558 and 1619 cm^{-1} in 7M6P-Mb (f) are distinct from those in spectrum b.

To confirm that the spectral change in 7M6P-Mb is due to changes in the hydrogen-bonding network, we changed the hydrogen-bonding partner of 7-propionate from Ser to Ala by site-directed mutagenesis. The results are shown in spectrum g. As expected, the overall features of spectra f and g are similar, but the effects of 7M6P and S92A on Y9a at 1177 cm^{-1} (spectra f and g, respectively) are slightly different: the S92A mutation (g) gives

rise to a derivative pattern at Y9a similar to that of NT Mb (b), whereas a small negative feature is observed for 7M6P-Mb (f).

2.2.5. Discussion

Conformational Changes in the *N-Terminus upon Ligand Binding* – There are two Trp residues in the A-helix of *sw*Mb. These residues can be used in UVRR spectroscopy to probe the conformational changes in the N-terminus upon ligand binding because they provide information about the protein tertiary structure in solution. We found that the intensity of the 229-nm-excited Trp7 signal is enhanced in the CO-bound form. On the other hand, binding of NO to the heme reduces the intensity of both Trp7 and Trp14 Raman bands. The intensities of the Trp bands are known to be sensitive to environmental hydrophobicity and/or hydrogen-bonding interactions of the Trp side-chain [18–20]. Because a frequency shift is not observed for the hydrogen bond marker band (877 cm^{-1}), we inferred that the hydrogen bonds between Trp7 or Trp14 and water molecules hardly change during the transition from the deoxy to the CO or NO-bound forms. Thus, it is reasonable to conclude that the hydrophobicity around only Trp7 changes upon CO binding, whereas the hydrophobicity around both Trp7 and Trp14 changes upon NO binding.

W7 mode is known as a marker for environmental hydrophobicity around Trp [18]. The ratio of the intensity of the W7 doublet bands (I_{1358}/I_{1340}) confirmed that the hydrophobicity around only Trp7 changes upon CO binding, whereas the hydrophobicity around both Trp7 and Trp14 changes upon NO binding. The higher frequency component (1359 cm^{-1}) of the W7 doublet is more intense in the CO-bound form and less intense in the NO-bound form. On the other hand, the intensity of the lower frequency component of W7 mode (1340 cm^{-1}) is unchanged in the CO- and NO-bound forms. Thus, the order of I_{1358}/I_{1340} is CO>deoxy>NO. Therefore, it is clear that Trp7 shifts to a more hydrophobic environment upon CO binding,

whereas Trp14 and Trp7 shift to a more hydrophilic environment upon NO binding. In addition, the Trp residues in the O_2-bound form show spectral changes close to those observed upon CO binding but significantly different from those of the NO-bound form, suggesting that the Trp environments become more hydrophobic upon O_2 binding.

The superimposition of three reported crystal structures for O_2-, CO- and NO-bound Mbs with the deoxy form [6–8] reveals that there is noticeable movement of the A-helix upon NO-binding (Fig.2.2.9), whereas there is a smaller movement upon CO or O_2 binding. The root-mean-square deviations (rmsd) of C_α atoms in A-helix (residues 4-18) with respect to deoxy form are 0.63, 0.08 and 0.29 Å for NO-, CO- and O_2-bound forms, respectively [the resolutions of crystal structures are 1.15 Å in deoxy (6), 1.7 Å in NO- (7), 1.15 Å in CO- (6), and 1.0 Å in O_2-bound forms (8) Mb]. The rmsd was calculated with Swiss-PdbViewer [21]. Considering the low resolution for NO-bound form, its rmsd value could be fluctuated. Nevertheless, the significant increment of rmsd in NO-bound form may suggest rather lager displacement from deoxy form. These observations are compatible with our results, in that Trp residues of the A-helix experience spectral changes four times larger upon NO binding than upon CO or O_2 binding. This implies a large tertiary structural change in the A-helix toward a more hydrophilic environment upon binding of NO and a smaller structural change toward a more hydrophobic environment upon binding of CO or O_2.

C-Terminal Conformational Changes upon Ligand Binding – The C-terminal region of the H-helix in *sw*Mb includes two Tyr residues, Tyr146 and Tyr151. A third tyrosine, Tyr103, is located in the G-helix. The UVRR results show that the Y9a band is upshifted in all the ligand-bound forms of Mb; however, the UVRR spectra of *h*Mb, which lacks Tyr151, does not show a shift in the frequency of Y9a for either the CO- [9] or NO-bound form. Thus, the frequency of the Y9a band of Tyr151 in *sw*Mb shifts upon ligand binding. In addition, the Y9a

frequency shift is coupled with an intensity decrease upon binding of O_2, as indicated by a positive peak at 1177 cm^{-1}. These results suggest that Tyr151 undergoes environmental changes upon binding of O_2, becoming a form that differs from the CO- and NO-bound forms, although the other Tyr residues (Tyr103 and Tyr146) may also make small contributions to the change in the intensity of the Y9a and Y8a bands in *sw*Mb.

Because the crystal structures show that Tyr103 is exposed to the solvent in all states [6–8], it is not expected that it contributes to the observed spectral changes. In contrast, Tyr146, which is embedded in a hydrophobic environment, is involved in the helix-loop interaction between the F-G loop and the H-helix by forming a hydrogen bond with the backbone of Ile99. Therefore, it is likely that Tyr146 also contributes to the spectral changes in Y9a for the NO- and O_2-bound forms and in Y8a for the CO-, NO-, and O_2-bound forms. This would confer changes in the hydrophobicity around C-terminal residues Tyr151 and Tyr146 or cause substantial alterations in their hydrogen bonding upon CO and NO binding.

Studies of Hb A have suggested that the change in the position of the C-terminal residue is physiologically important. Specifically, removal of the C-terminal residue in the α (Arg141) or β (His146) subunit locks the tetramer in the R state and eliminates cooperativity [22,23]. This means that ligand binding to one subunit is communicated to other subunits via the C-terminal residue. Given this information, it is reasonable that Tyr151 exhibits structural changes upon ligand binding. It is interesting that this structural change varies according to the ligand because the cooperativity of Hb also depends on the ligand.

Transmission of Structural Changes from Heme to the N-terminus upon CO or NO Binding – To understand how the conformational changes are transmitted from heme to the N- and C-termini upon CO and NO binding, we monitored the changes in the UVRR spectra of the aromatic residues in forms of Mb in which one of the predicted pathways (His93,

6-propionate, or 7-propionate) was eliminated by mutation or chemical modification of heme. The H93G (+Imd) mutant serves as a mimic of NT Mb in which the covalent bond between heme and globin is cleaved and an exogenous imidazole binds to iron freely in the proximal cavity [13]. The sub-picosecond time-resolved RR spectra showed ultra-rapid heme doming following ligand dissociation in this cavity mutant, suggesting that the out-of-plane movement of iron is independent of its chemical linkage to His93 in NT Mb [11]. This left the question of whether this covalent bond is responsible for communication between the heme and the protein moiety. Unexpectedly, the UVRR difference spectra of H93G(+Imd) Mb are very similar to those of NT Mb upon CO and NO binding, despite the absence of a covalent bond between the heme and globin. This strongly suggests that the Fe-His93 bond is not directly responsible for transferring the structural changes from the heme to the A-helix upon CO or NO binding.

As shown in Fig.2.2.1, the 6-propionate side-chain of heme is directed to the distal side of heme and forms a hydrogen bond with Arg45. In the case of CO binding, Trp7 of 6M7P-Mb, which lacks the 6-propionate, shows environmental changes similar to those of NT Mb, suggesting that the hydrophobic environment around the A-helix in NT and 6M7P Mbs are similar. On the other hand, binding of NO to the R45L mutant, in which the hydrogen bond between Arg45 and 6-propionate is removed, displays negative bands, whereas NT Mb shows positive peaks. These results suggest that, as in the S92A mutant, the environment of the A-helix in the R45L mutant changes from hydrophilic to hydrophobic upon NO binding.

The crystal structures show that the Fe-C-O binding geometry is nearly linear and that its oxygen atom is 3.21 Å away from the Nε of His64, indicating a very weak hydrogen bond [6]. In contrast, Fe-N-O shows a bent geometry with an angle of 112°, and its nitrogen atom is 2.78 Å away from the Nε of His64 [7], indicating a stronger hydrogen bond. Fig.2.2.1 shows that the distal His64 is involved in the hydrogen-bonding network with Arg45 and 6-propionate through a water molecule. Regarding the strength of the electrostatic field, which is modulated

by NO or CO, the elimination of the hydrogen bond between the 6-propionate and Arg45 could disrupt the distal pocket in the NO-bound form more significantly than in the CO-bound form. This structural feature is compatible with our present results showing that the 6-propionate is important for transmitting the conformational changes from heme to the N-terminus upon NO binding.

Fig2.2.1 shows that the 7-propionate side-chains of heme form hydrogen bonds with Ser92 and His97. The spectral changes upon binding of CO to 7M6P- or S92A Mb are significantly different than those for NT. In addition, for the S92A mutant, NO binding causes mainly negative peaks in the difference spectrum, whereas that for NT shows positive peaks. Thus, the disruptions of the 7-propionate hydrogen-bonding network in the proximal side affect the conformational change in the N-terminal region upon CO or NO binding. The presence of a Ser or Thr at the F7 position in mammalian Mbs is highly conserved, and they form stable hydrogen bonds with nitrogen of the proximal His93 and the 7-propionate hydroxyl group, although such hydrogen bonds are not present at the F7 position of the α- and β-chains of Hb A [24]. Replacement of Ser92 with Ala, Val, or Leu causes disorder in the heme pocket [25-27]. In spite of the disorder in the geometry, the kinetic data show only a slight increase in the association rate for CO and an essentially unaltered dissociation rate [25,26]. Our finding is consistent with these results, in that the proximal hydrogen bonds are not only essential for maintaining the protein structure but also for transmitting the heme conformational changes to the globin moiety.

Transmission of Structural Changes of Heme to the C-terminus upon CO Binding – As mentioned above, the UVRR results showed that the environment around Tyr151 in the C-terminus changes upon ligand binding. In contrast, the spectral changes for 6M7P- and R45L mutants are similar to those in NT Mb, indicating that the distal hydrogen bonds are not

responsible for transmitting structural changes to the C-terminus. On the contrary, the spectra for 7M6P- and S92A Mb exhibit significant changes in the Y8a band (1619 cm^{-1}), suggesting a difference in the communication through the 7-propionate. In particular, the dissimilar patterns at Y9a between 7M6P- and S92A Mb could be due to the absence of the hydrogen bond between the 7-propionate and His97 in 7M6P-Mb (see Fig.2.2.1). Consequently, the absence of one of the hydrogen bonds between the 7-propionate and both Ser92 and His97 significantly perturbs the transmission of the structural change from heme to the C-terminus. Thus, the hydrogen bonds between the 7-propionate and the F-helix regulate the changes in protein conformation that take place upon CO binding.

Role of Heme-propionate Side-chains in Heme Sensor Proteins – In heme-based sensor proteins, the conformational changes induced by binding of a gas molecule to the heme in the sensor domain modulate the activity of the functional domain. A central issue is how the heme structural changes initiated by binding of a gas molecule are propagated to the environment around the heme and, further, to the functional domain. The FixL proteins, which contain a histidine kinase domain that is regulated by oxygen binding, discriminate between O_2, NO, and CO and switch to the inactive state only upon binding of O_2 [28,29]. X-ray data for *Bj*FixLH reveal that the binding of O_2 forces Arg220 to rupture its salt bridge to the 7-propionate in the unligated (ferric/deoxy) state and then to move to the distal heme pocket and form a hydrogen bond with O_2. Subsequently, Arg206 forms a hydrogen bond with the released 7-propionate. In contrast, the binding of NO and CO does not cause such an alteration in the salt bridge [30]. Similarly, the 7-propionate plays an important role in the intramolecular signaling of the direct oxygen sensor protein, *Ec* DOS. Specifically, the hydrogen-bonding network between 7-propionate, Arg97, and heme-coordinated O_2 in *Ec* DOS is replaced by a hydrogen bond between the 7-propionate and the heme axial ligand (Met95) upon reduction [31]. Furthermore,

the RR spectra reveal that the frequency of the propionate bending mode [$\delta(C_\beta C_c C_d)$], which is indicative of hydrogen bonding of the heme propionate [32], is located at 383 cm^{-1} in the O_2-bound form but at 379 cm^{-1} in the CO-bound form [33], implying that the 7-propionate hydrogen-bonding network is different for the O_2 and CO forms.

The ability of Mb to discriminate ligands is related to the ligand affinities. Practically, the electrostatic interactions between the bound ligand and the distal His along with the steric hindrance within the heme pocket [34,35] regulate the ligand affinity. Our work demonstrates that such interactions in the heme site could influence the conformational changes in the terminal regions of the protein. In addition, some changes in the hydrogen bonds between two propionate side chains and ambient residues are involved in the process of ligand binding and play distinct roles for different ligands. This kind of interaction seems to be significant for ligand discrimination by *Bj*FixLH [28-30] and *Ec*DosH [33,36]. Based on this common viewpoint, transmission of the structural changes from heme to protein in Mb could reveal some essential aspects of the intramolecular signal transduction by heme-based sensor proteins.

In conclusion, the UVRR difference spectra selectively detected that there are changes in the environments around the Tyr residues in C-terminal and Trp residues in N-terminal of *sw*Mb upon binding of O_2, CO, and NO to the heme iron. The conformational changes in these two regions are parts of conformational changes which occur in the whole protein of *sw*Mb. Our results show that the heme discriminates between different ligands by inducing significantly different protein conformational changes in the A- and H-helices. Furthermore, we showed the roles of the Fe-His and heme propionates in communicating the conformational changes to the N- and C-termini.

References:

1. Perutz, M. F., Fermi, G., Luisi, B., Shaanan, B., and Liddington, R. C. (1987) *Acc. Chem. Res.* **20**, 309

2. Rodgers, K. R. (1999) *Curr. Opin. Chem. Biol.* **3**, 158

3. Aono, S., and Nakajima, H. (1999) *Coord. Chem. Rev.* **190-192**, 267

4. Chan, M. K. (2000) *Nat. Struct. Biol.* **7**, 822

5. Takano, T. (1977) *J. Mol. Biol.* **110**, 569

6. Kachalova, G. S., Popov, A. N., and Bartunik, H. D. (1999) *Science* **284**, 473

7. Brucker, E. A., Olson, J. S., Ikeda-Saito, M., and Phillips, G. N. Jr. (1998) *Proteins.* **30**, 352

8. Vojtechovsky, J., Chu, K., Berendzen, J., Sweet, R. M., and Schlichting, I. (1999) *Biophys.J.* **77**, 2153

9. Haruta, N., Aki, M., Ozaki, S., Watanabe, Y., and Kitagawa, T. (2001) *Biochemistry* **40**, 6956

10. Mizutani, Y., and Kitagawa, T. (2001) *Chem. Rec.* **1**, 258

11. Franzen, S., Bohn, B., Poyart, C., DePillis, G., Boxer, S. G., and Martin, J.-L. (1995) *J. Biol. Chem.* **270**, 1718

12. Springer, B. A., Egeberg, K. D., Sligar, S. G., Rohlfs, R. J., Mathews, A. J., and Olson, J. S. (1989) *J. Biol. Chem.* **264**, 3057

13. Barrick, D. (1994) *Biochemistry* **33**, 6546

14. Hayashi, T., Nakagawa. T., Harada, K., Matsuo, T., Hitomi, Y., and Hisaeda, Y. (2004) *Chem. Lett.* **33**, 1512

15. Hauksson, J. B., La Mar, G. N., Pandey, R. K., Rezzano, I. N., and Smith, K. M. (1990) *J. Am. Chem. Soc.* **112**, 6198

16. Aki, M., Ogura, T., Shinzawa-Itoh, K., Yoshikawa, S., and Kitagawa, T. (2000) *J. Phys. Chem. B* **104**, 10765

17. Harada, I. and Takeuchi, H. (1986) In *Spectroscopy of Biological Systems, Advances in Spectroscopy*; Clark, R. J. H., Hester, R. E., Eds., John Wiley & Sons, New York **13**, 113

18. Takeuchi, H. (2003) *Biopolymers* **72**, 305

19. Rodgers, K. R., Su, C., Subramaniam, S., Spiro, T. G. (1992) *J. Am. Chem. Soc.* **114**, 3697

20. Austin, J. C., Jordan, T., and Spiro, T. G. (1993) in *Biomolecular Spectroscopy, Part A* (Clark, R. J. H., and Hester, R. E., eds), **20**, pp. 55 - 127, John Wiley & Sons, New York

21. Guex, N. and Peitsch, M. C. (1997) *Electrophoresis* **18**, 2714

22. Kilmartin, J. V., Imai, K., Jones, R. T., Farqui, A. R., Fogg, J, and Baldwin, J. M. (1978) *Biochim. Biophys, Acta* **534**, 15

23. Fung, L. W. –M. and Ho, C (1975) *Biochemistry* **14**, 2526

24. Bashfold, D., Chothia, C., and Lesk, A.M. (1987) *J. Mol. Biol.* **196**, 199

25. Shiro, Y., Iizuka, T., Marubayashi, K., Ogura, T., Kitagawa, T., Balasubramanian, S., and Boxer, S G. (1994) *Biochemistry* **33**, 14986

26. Smerdon, S. J., Krzywda, S., and Wilkinson, A. J. (1993) *Biochemistry* **32**, 5132

27. Peterson, E. S., Friedman, J. M., Chien E. Y. T., and Sligar, S. G. (1998) *Biochemistry* **37**, 12301

28. Tuckerman, J. R., Gonzalez, G., Dioum, E. M., and Gilles-Gonzalez, M.-A. (2002) *Biochemistry* **41**, 6170

29. Dunham, C. M., Dioum, E. M., Tuckerman, J. R., Gonzalez, G., Scott, W. G., and Gilles-Gonzalez, M.-A. (2003) *Biochemistry* **42**, 7701

30. Hao, B., Isaza, C., Arndt, J., Soltis, M., and Chan, M. K. (2002) *Biochemistry* **41**, 12952

31. Park, H., Suquet, C., Satterlee, J. D., and Kang, C. (2004) *Biochemistry* **43**, 2738

32. Cerda-Colon, J. F., Silfa, E., and Lopez-Garriga, J. (1998) *J. Am. Chem. Soc.* **120**, 9312

33. Sato, A., Sasakura, Y., Sugiyama, S., Sagami, I., Shimizu, T., Mizutani, Y., and Kitagawa, T. (2002) *J. Biol. Chem.* **277**, 32650

34. Springer, B. A., Sligar S. G., Olson, J. S. and Phillips, G. N., Jr. (1994) *Chem. Rev.* **94**. 699

35. Spiro, T. G., and Kozlowski, P. M. (2001) *Acc. Chem. Res.* **34**, 137

36. Uchida, T., and Kitagawa, T. (2005) *Acc. Chem. Res.* **38**, 662

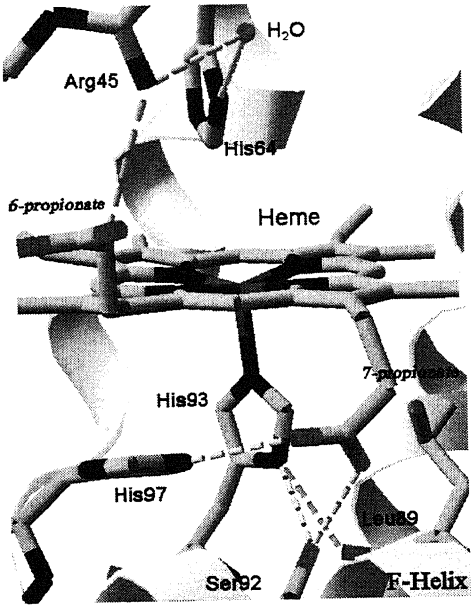

Fig.2.2.1. Hydrogen-bonding network in the vicinity of heme of *sw*Mb. (Taken from Ref. 6)

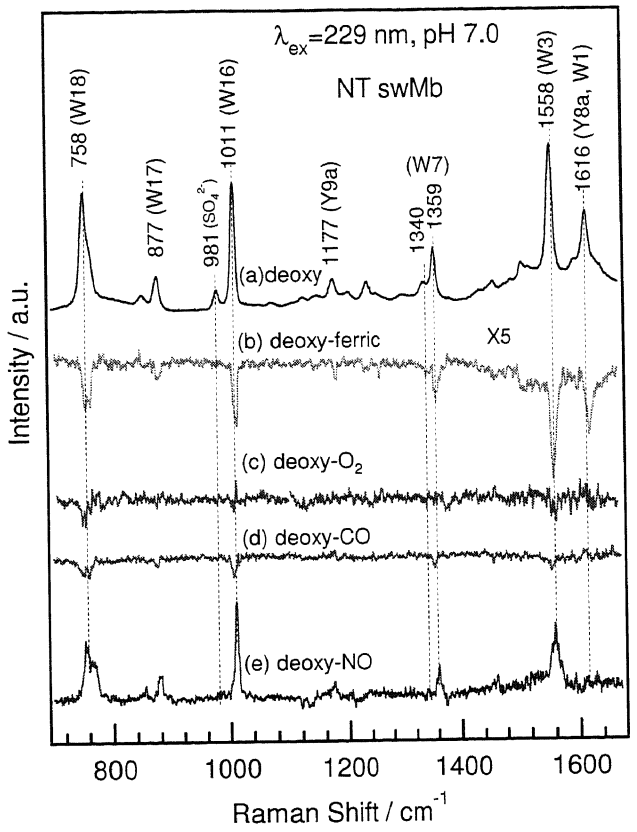

Fig.2.2.2. The 229-nm excited UVRR spectra of NT *sw*Mb. Showns are the spectrum for the deoxy form of NT Mb (a) and the following difference spectra for NT Mb: (b) deoxy – ferric, (c) deoxy – O_2, (d) deoxy – CO, and (e) deoxy – NO. The sample concentration was 200 μM in 50 mM phosphate buffer, pH 7.0. 400 mM Na_2SO_4 was used as an internal intensity standard

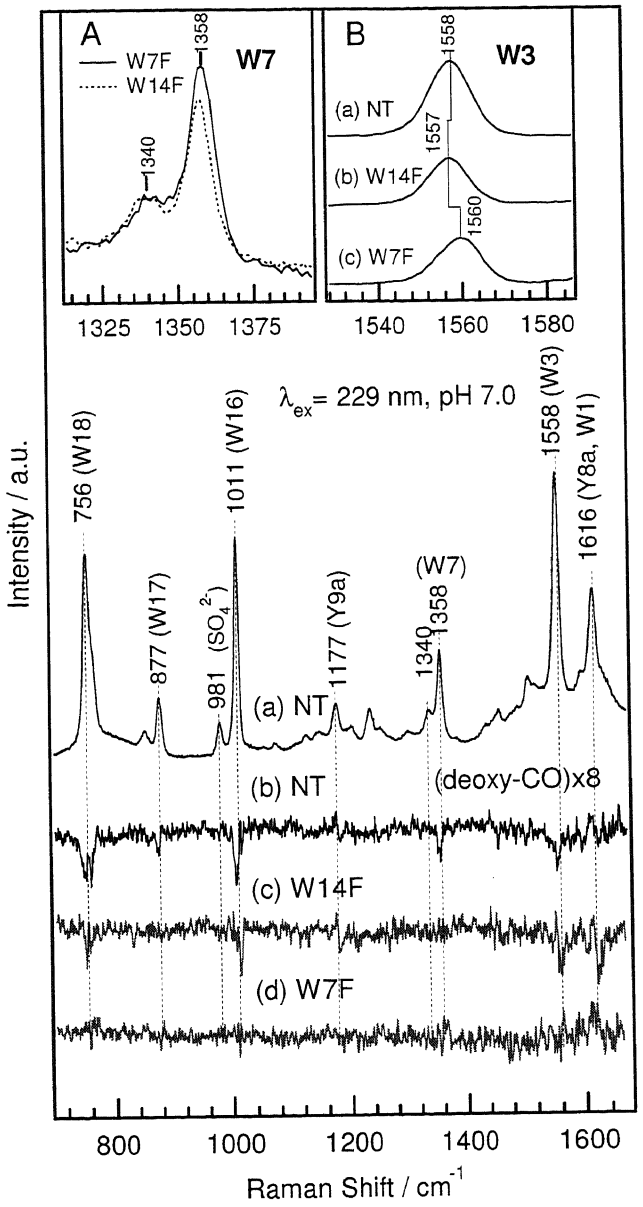

Fig.2.2.3. The 229-nm excited UVRR spectra of NT and Trp mutants of *sw*Mb. Showns are the spectrum for the deoxy form of NT Mb (a) and the deoxy – CO difference spectra for NT Mb (b) and the W14F- (c) and W7F-Mb (d). Insets show the enlarged raw spectra of the W7 (A) and W3 modes (B). The sample concentration was 200 μM in 50 mM phosphate buffer, pH 7.0. 400 mM Na_2SO_4 was used as an internal intensity standard.

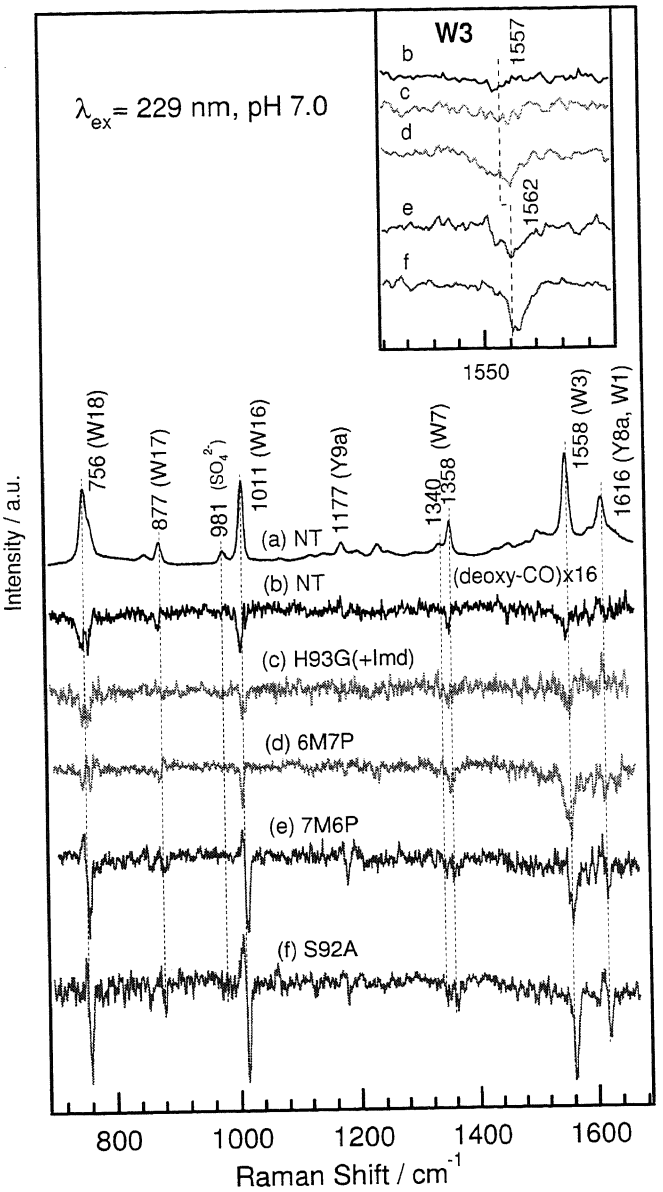

Fig.2.2.4. The 229-nm excited UVRR spectra of NT, mutant, and modified heme *sw*Mbs. Showns are the spectrum for the deoxy form of NT Mb (a) and the deoxy – CO difference spectra for NT Mb (b) and the H93G(+Imd) (c), 6M7P- (d), 7M6P- (e), and S92A (f) forms of Mb. The inset shows the enlarged difference spectra of W3 mode. The sample concentration was 200 μM in 50 mM phosphate buffer, pH 7.0. 400 mM Na_2SO_4 was used as an internal intensity standard.

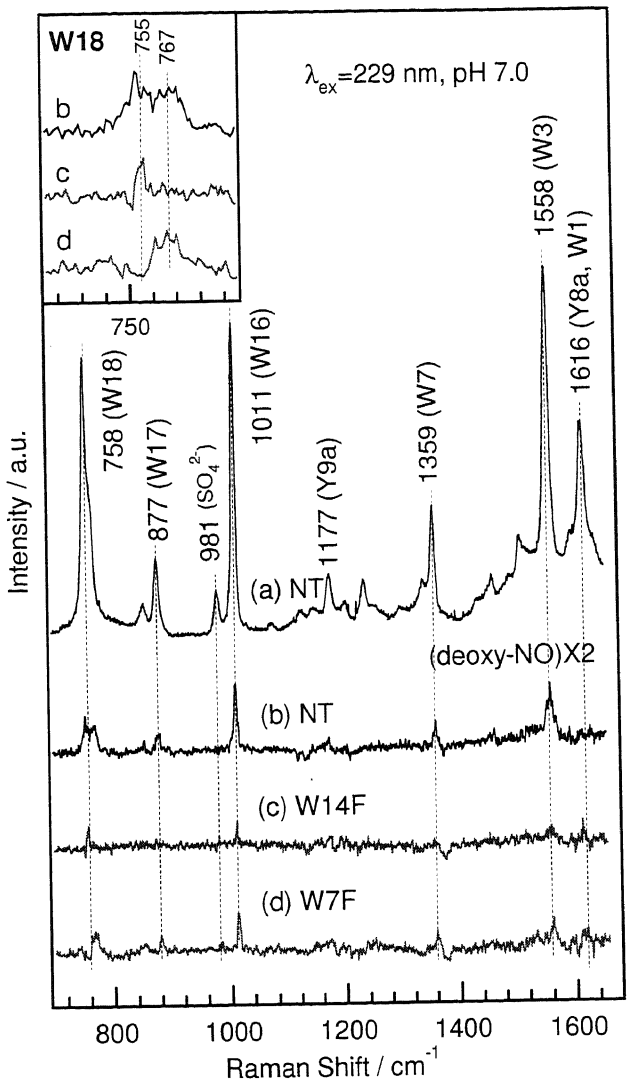

Fig.2.2.5. The 229-nm excited UVRR spectra of NT and Trp mutants of *sw*Mb. Showns are the spectrum for the deoxy form of NT Mb (a) and the difference spectra (deoxy – NO) of NT Mb (b) and the W14F- (c) and W7F-Mb (d). The inset shows the enlarged difference spectra of W18 mode. The sample concentration was 200 μM in 50 mM phosphate buffer, pH 7.0. 400 mM Na_2SO_4 was used as an internal intensity standard.

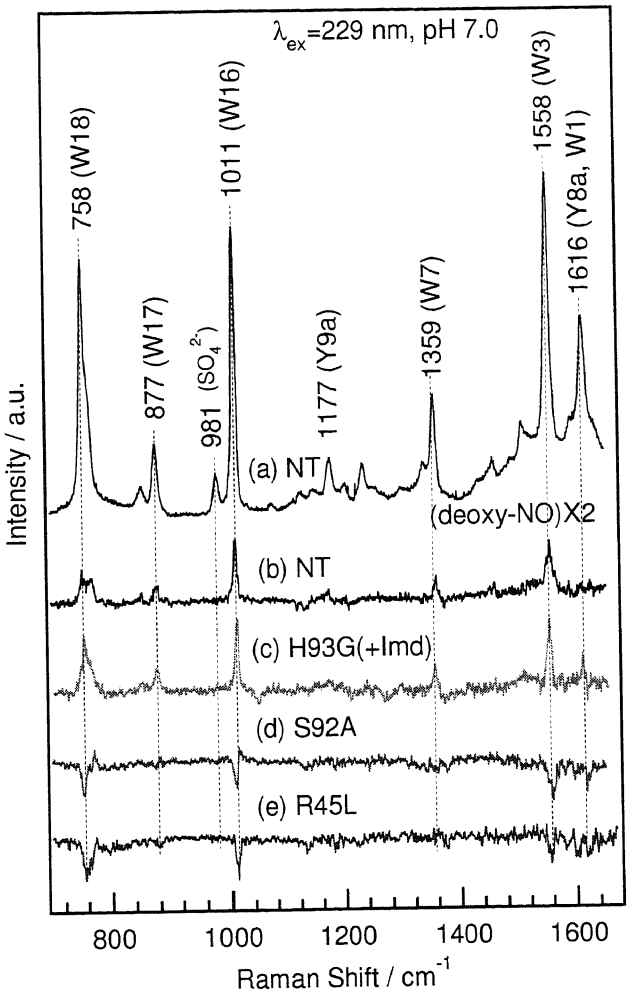

Fig.2.2.6. The 229-nm excited UVRR spectra of NT and mutant *sw*Mbs. Showns are the spectrum for the deoxy form of NT Mb (a) and the deoxy – NO difference spectra for NT Mb (b) and the H93G(+Imd) (c), S92A (d), and R45L (e) forms of Mb. The sample concentration was 200 μM in 50 mM phosphate buffer, pH 7.0. 400 mM Na_2SO_4 was used as an internal intensity standard.

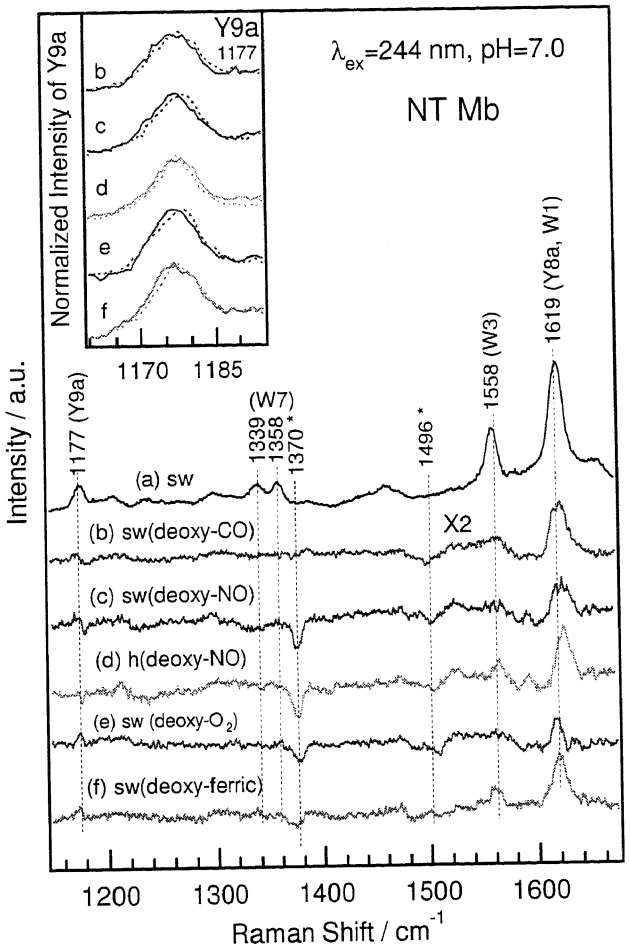

Fig.2.2.7. The 244-nm excited UVRR spectra of NT *sw*Mb and *h*Mb. Showns are the spectrum for the deoxy form of *sw*Mb (a) and the following difference spectra: (b) deoxy – CO of *sw*Mb, (c) deoxy – NO of *sw*Mb, (d) deoxy – NO of *h*Mb, (e) deoxy – O_2 of *sw*Mb, and (f) deoxy – ferric of *sw*Mb. The asterisks indicate the Raman bands of heme. The inset shows the enlarged raw spectra of the Y9a mode in the intensity normalized specta. The deoxy (solid line) and ligand-bound forms (dotted line) overlapped. The sample concentration was 300 μM in 50 mM phosphate buffer, pH 7.0. 100 mM Na_2SO_4 was used as an internal intensity standard.

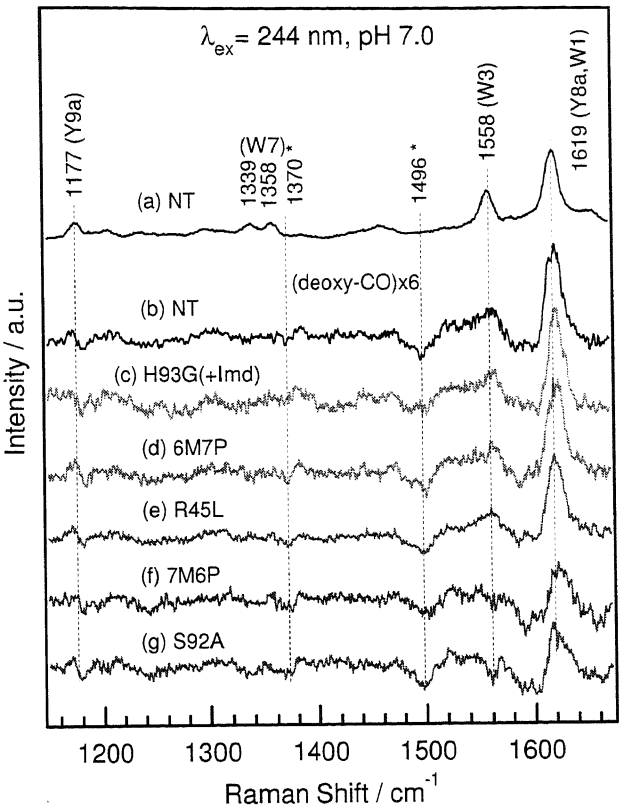

Fig.2.2.8. The 244-nm excited UVRR spectra of NT, mutant, and modified heme *sw*Mbs. Showns are the spectrum for the deoxy form of NT Mb (a) and the deoxy – CO difference spectra of NT Mb (b) and the H93G(+Imd) (c), 6M7P- (d), R45L (e), 7M6P- (f), and S92A (g) forms of Mb. The asterisks indicate the Raman bands of heme. The sample concentration was 300 μM in 50 mM phosphate buffer, pH 7.0. 100 mM Na_2SO_4 was used as an internal intensity standard.

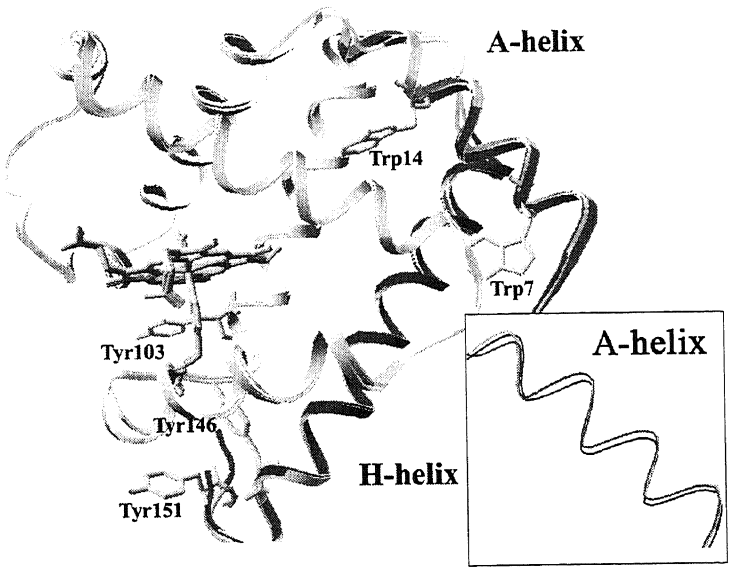

Fig.2.2.9. Superimposition of crystal structures of NT *sw*Mb in the deoxy form and the CO-, NO-, and O_2-bound forms. The highlighted parts indicate the A- and H-helices. The inset shows the enlarged A-helix region. The deoxy (green; 1BZP), CO-bound (orange; 1BZR), NO-bound (purple; 1HJT), and O_2-bound forms (red; 1A6M) are superimposed. (Taken from refs. 6–8)

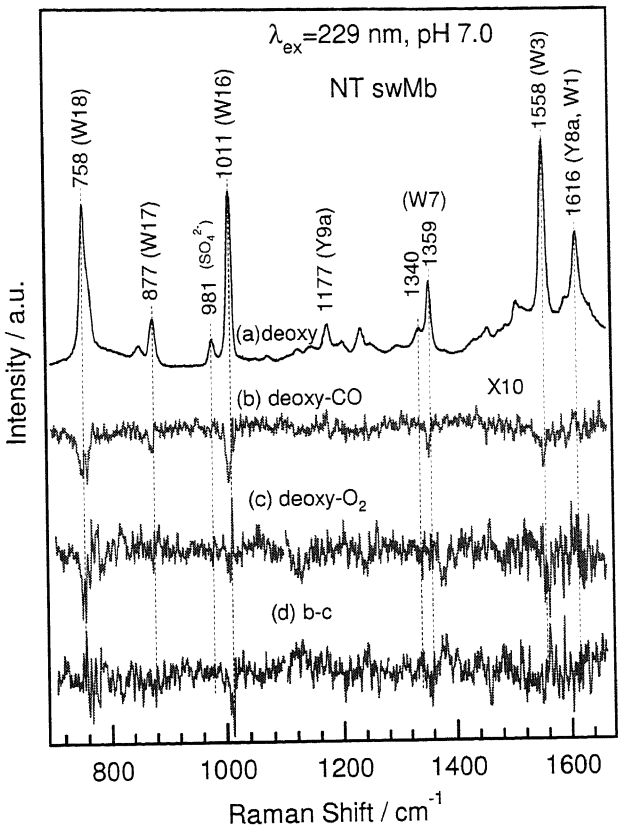

Fig.S2.2.1 The 229-nm excited UVRR spectra of NT *sw*Mb. Showns are the spectrum for the deoxy form of NT Mb (a) and the following difference spectra for NT Mb: (b) deoxy – CO, (c) deoxy – O_2, and (d) b – c. The sample concentration was 200 μM in 50 mM phosphate buffer, pH 7.0. 400 mM Na_2SO_4 was used as an internal intensity standard.

Chapter 3. Vibrational Energy Relaxation in Heme "Cooling"

(Chem. Phys. Lett. 2006, 429, 239-243)

3.1. Overview of Techniques Utilized for Monitoring the Vibrational Energy Relaxation

Vibrational energy relaxation and dispersion on an intermolecular level play an important role in determining the channel of energy flow following the photo-trigger reactions. MbCO has been studied extensively from the energetic and dynamic standpoint as a well characterized model system. One advantage for Mb is that the dynamic process from ligated to unligated form Mb can be triggered by photo within 50 fs time regime with quantum yield of nearly unit [1-4]. Another advantage is the recombination of CO to unligated Mb is much slower compared with that of O_2 or NO, therefore the complicated side reactions and associated population dynamics can be avoided [5]. These characters of MbCO allow optical probes to follow the ultrafast process of intramolecular vibrational redistribution within the Mb and the intermolecular energy transform from the hot Mb to the surrounding solvent. Several ultrafast techniques have been used to capture such energy relaxation and protein dynamic process, including transient phase grating spectroscopy [6-9], reaction kinetics experiments [10,11] , time-resolved IR spectroscopy [12-15] and resonance Raman spectroscopy [16-20].

The transient phase grating spectroscopy detects the photoinduced changes in index of refraction, therefore, is sensitive to the density changes [21]. Density changes can occur through atomic displacement which is caused by either thermal expansion or systematic motions of protein matrix. The vibrational energy transfer from the porphyrin ring to solvent has been detected by monitoring the solvent lattice

temperature by this technique [21,22]. Also the protein motions and volume changes following CO photolysis have been investigated by the grating spectroscopy [9].

The rate of ligand rebinding to Mb after CO photolysis has been investigated extensively and the kinetic data has been fitted by various models [10,11,23,24]. The AH model simplified the ligand/protein/solvent complex to two coordinates, the ligand rebinding coordinate and the protein coordinate. The latter is modeled by the overdamped diffusive dynamics with an associated diffusion constant that depends on the temperature and solvent type [11]. However the definite character of protein coordinate is not so clear.

Time-resolved IR and Raman spectroscopy can provide more direct information and much higher resolution of vibrational population. A femtosecond IR experiment has been performed to study the heating of D_2O after CO dissociated from heme proteins by monitoring the shift of infrared absorption band of water [12]. Also by using ultrafast IR, the relaxation time for unligated protein has been investigated by examing the amide bands of protein polypeptide [25-27]. However, it is still hard to measure a wide frequency ranges in IR spectroscopy, due to the interference of water bands. On the contrary, time-resolved Raman spectroscopy can provide many vibrational transitions in a wide frequency range with single probe frequency. Another advantage of Raman spectroscopy is that the integrated areas of anti-Stokes to Stokes ratio serves as an ideal probe for determining the local vibrational temperature of excited modes, after corrected to the first order for reabsorption and cross section differences [17,28].

In this chapter, heme propionate side chains were investigated from the viewpoint of energy relaxation in Mb following CO photolysis, by using the time-resolved anti-Stokes Raman spectroscopy.

References:

1. Bucher, T., and Kaspers, J. (1947) *Biochim. Biophys. Acta* **1**, 21
2. Schuresko, D. D., and Webb, W. W. (1978) *Biophys. J.* **24**, 382
3. Greene, B. I., Hochstrasser, R. M., Weisman, R. B., and Eaton, W. A. (1978) *Proc. Natl. Acad. Sci. U. S. A.* **75**, 5255
4. Petrich, J. W., Poyart, C., and Martin, J. L. (1988) *Biochemistry* **27**, 4049
5. Gibson, Q. H., Olson, J. S., McKinnie, R. E., and Rohlfs, R. J. (1986) *The Journal of biological chemistry* **261**, 10228
6. Richard, L., Genberg, L., Deak, J., Chiu, H. L., and Miller, R. J. D. (1992) *Biochemistry* **31**, 10703
7. Miller, R. J. D. (1994) *Acc. Chem. Res.* **27**, 145
8. Deak, J., Richard, L., Pereira, M., Chui, H. L., and Miller, R. J. D. (1994) *Methods Enzymol.* **232**, 322
9. Miyata, R., and Terazima, M. (2003) *Bull. Chem. Soc. Jpn.* **76**, 1707
10. Frauenfelder, H., and Wolynes, P. G. (1985) *Science* **229**, 337
11. Agmon, N., and Hopfield, J. J. (1983) *J. Chem. Phys.* **79**, 2042

12. Lian, T., Locke, B., Kholodenko, Y., and Hochstrasser, R. M. (1994) *J. Phys. Chem.* **98**, 11648

13. Owrutsky, J. C., Li, M., Locke, B., and Hochstrasser, R. M. (1995) *J. Phys. Chem.* **99**, 4842

14. Hill, J. R., Tokmakoff, A., Peterson, K. A., Sauter, B., Zimdars, D., Dlott, D. D., and Fayer, M. D. (1994) *J. Phys. Chem.* **98**, 11213

15. Sagnella, D. E., Straub, J. E., Jackson, T. A., Lim, M., and Anfinrud, P. A. (1999) *Proc. Natl. Acad. Sci. U. S. A.* **96**, 14324

16. Mizutani, Y., and Kitagawa, T. (2001) *Chem. Rec.* **1**, 258

17. Schomacker, K. T., Bangcharoenpaurpong, O., and Champion, P. M. (1984) *J. Chem. Phys.* **80**, 4701

18. Shreve, A. P., and Mathies, R. A. (1995) *J. Phys. Chem.* **99**, 7285

19. Mizutani, Y., and Kitagawa, T. (1997) *Science* **278**, 443

20. Mizutani, Y., and Kitagawa, T. (2001) *J. Phys. Chem. B* **105**, 10992

21. Genberg, L., Heisel, F., McLendon, G., and Miller, R. J. D. (1987) *J. Phys. Chem.* **91**, 5521

22. Miller, R. J. D. (1991) *Annu. Rev. Phys. Chem.* **42**, 581

23. Ando, K., and Sumi, H. (2003) *The Journal of Chemical Physics* **118**, 8315

24. Schlichter, J., Friedman, J., Herenyi, L., and Fidy, J. (2000) *J. Chem. Phys.* **112**, 3045

25. Xie, X., and Simon, J. D. (1991) *Biochemistry* **30**, 3682

26. Xie, A., Van Der Meer, L., Hoff, W., and Austin, R. H. (2000) *Phys. Rev. Lett.* **84**, 5435

27. Causgrove, T. P., and Dyer, B. R. (1996) *J. Phys. Chem.* **100**, 3273

28. Okamoto, H., Nakabayashi, T., and Tasumi, M. (1997) *J. Phys. Chem. A* **101**, 3488

3.2. Time-resolved Raman Evidence for Energy "Funneling" through Propionate Side Chains in Heme "Cooling" upon Photolysis of Carbonmonoxy Myoglobin

3.2.1. Abstract:

The heme "cooling" following CO photolysis was investigated with picosecond time-resolved anti-Stokes Raman spectroscopy on modified Mbs, in which the 6- or 7-propionate is selectively replaced by a methyl group. The time constants of population decay of vibrationally excited states for two modified Mbs became significantly larger compared with those of native Mb. This is the first experimental evidence for appreciable contribution of each heme-propionate side chain to the vibrational energy transfer from the heme to the surroundings.

3.2.2. Introduction

Studies on vibrational energy relaxation in proteins are important to characterize ultrafast processes of photoreactions. Regarding heme proteins, the axial gaseous ligand is photodissociated by a visible light and at the same time the remaining deligated heme is vibrationally excited. The relaxation of vibrationally excited heme will induce energy redistribution within the heme and finally dissipation into the surrounding solvent and protein matrix. The time scale and mechanisms for "cooling" of heme following the ligand photolysis have been investigated by computer simulation as well as ultrafast spectroscopy [1-12]. Molecular dynamic simulation studies indicated a fast "cooling" process within 10 ps time scale [1-4]. Time-resolved resonance Raman (TR^3) and infrared studies of heme proteins in solution have revealed the occurrence of heme vibrational relaxation in a few picoseconds time regime [7-9]. In our previous study, the population relaxation of in-plane vibrational modes of heme following CO photodissociation from MbCO was monitored by using time-resolved anti-Stokes Raman spectroscopy, and time constants of 1.1± 0.6 and 1.9 ±0.6 ps were obtained for the decays of ν_4 and ν_7, respectively [10,11]. In Mb, the heme is embedded in the protein matrix and the contacts between heme and globin are mainly nonpolar, with the exception of the two heme-propionate side chains protruding into the solvent and forming hydrogen bonds with the protein residues (Arg45, Ser92 and His97). It is reported that replacement of heme with a porphin slows the vibrational relaxation [12], while only 17% of heat energy is dissipated into solvent water directly [13]. The molecular dynamic

simulation studies suggested that the highly solvated propionate side chains seem to be the "doorway" for dissipation of the excess energy in the heme [3,4]. However, there has been no direct experimental evidence for it.

To address this issue, we applied picosecond-TR^3 (ps-TR^3) anti-Stokes spectroscopy to four kinds of *sw*Mb samples and monitored the vibrational energy relaxation following CO photolysis. The samples include two modified heme-containing Mbs, in which the 6- or 7-propionate side chain was selectively replaced by a methyl group, and two Mb mutants, in which the hydrogen bond between either of propionate side chains and protein residue was eliminated by a site-directed mutagenesis. The time constants of energy relaxation obtained from them were compared with that from the NT *sw*Mb. The results indicate that the heme-propionate side chains are highly involved in the energy transfer from the heme to the surroundings, while the hydrogen bonds between the propionate and protein contribute to it little.

3.2.3. Experimental

The details of the ps-TR^3 apparatus are described elsewhere [11]. Briefly, a picosecond mode-locked Ti:sapphire laser system produced approximately 2.7 ps pulses of 784 nm. A 540-nm pump pulse was generated with a home-built optical parametric generator (OPG) and amplifier (OPA) from the 784 nm pulse. A probe pulse at 442 nm was generated as the first Stokes stimulated Raman scattering from compressed methane gas (50 kg/cm^2) excited by the second harmonic of the 784 nm

output. The pump and probe beams were made collinear and coaxial using a dichroic mirror. The polarization of the pump beam was rotated by 55° relative to that of the probe beam to minimize the effects of molecular rotations on the observed kinetics. The laser power at the sample point was 10 and 0.1 μJ for the pump and probe beams, respectively. A cross correlation trace of the pump and probe pulses was measured with a 1-mm BBO crystal, which indicated a width of 2.3 ps. The 0.0 ps of delay time (Δt, uncertainty < 0.2 ps) was calibrated using sum frequency mixing in the same crystal.

The sample solution was contained in a 10 mmϕ NMR tube and spun at 3400 rpm with the home-made spinning cell device. Spherical and cylindrical lenses were used to focus the pump and probe beams on the sample. Raman signal was collected at 135° back-scattering [14] and imaged onto the 200-μm entrance slit of a single spectrometer (Spex, 500M). A holographic notch filter was used to reject the unshifted scattering. Finally, the scattered light was detected by a liquid nitrogen-cooled CCD detector (Roper Scientific, Spec-10:400B/LN). Raman shifts were calibrated with cyclohexane, benzene, or carbon tetrachloride. The peak positions of Raman bands are accurate within ±2 cm^{-1}. Data acquisition was described elsewhere [11].

NT *sw*Mb (Biozyme) was used without further purification. Mb mutants including S92A, and R45L were expressed and purified as described previously [15]. Chemically modified hemes in which the 7- (7Me) or 6-propionate (6Me) of protoporphyrin IX was replaced by a methyl group were synthesized as described

elsewhere [16]. The Fe(III) complexes were reconstituted into the *sw*Mb apoprotein [17]. The correct cooperation between heme and protein was identified (see section: Appendix). For ps-TR^3 measurements, the concentration of protein was adjusted to 100 μM in 50 mM phosphate buffer at pH 7.0. About 1 mL of the Mb solution was put into an airtight NMR tube. For MbCO, the sample was reduced by sodium dithionite after degassing and back-filling with CO. The sample was replaced with a fresh one every 3 hours. Sample integrity was confirmed with UV-vis absorption spectra after the ps-TR^3 measurements.

3.2.4. Results and Discussion

TR^3 anti-Stokes spectroscopy is selective for vibrationally excited modes, and it is therefore a powerful tool for measuring vibrational energy relaxation [18-20]. The anti-Stokes TR^3 spectra of NT *sw*Mb between -5 ps to 50 ps with 2.3-ps resolution, which are represented as differences of the pump-probe spectra minus the probe-only spectrum after intensity correction with the raw spectra, are displayed in Fig.3.2.1, where the delay times of the probe pulse from the pump pulse are specified at the edge of each spectrum. The difference spectrum reflects solely the photoproduct of Mb after CO dissociation [11]. The anti-Stokes intensities are highest at 1-ps delay, when the in-plane vibrational modes of heme are observed at 670, 784, 1123, 1354 and 1465 cm^{-1}. These bands are assigned to ν_7, ν_6, ν_5, ν_4, and ν_3, respectively (Fig.3.2.1) [21,22]. The slightly altered peak frequencies (Fig.3.2.2) compared with those in the previous study arise from the usage of different Mbs (*sw*Mb in this work,

while horse Mb in the previous study). The intensities of these bands decrease as the delay time increases, and approach the equilibrium within 10-ps delay. The ratio of the integrated areas of anti-Stokes to Stokes scattering is expected to provide the most direct information about relative vibrational population [20,23]. Since there is no significant intensity changes with the evolution of time in the Stokes ν_7 and ν_4 bands as revealed previously [10] , the considerable intensity decay of the anti-Stokes ν_7 and ν_4 bands observed here can be attributed to the vibrational energy relaxation of the excited heme after CO photodissociation. In order to identify the function of heme propionate side chains in the process of the vibrational energy dissipation, similar experiments are performed for the 7Me- and 6Me-*sw*Mb. The anti-Stokes TR^3 difference spectra of 7Me- and 6Me-*sw*Mb with time delay from -5 ps to 50 ps are shown in Fig.3.2.4 and 3.2.3. The observed frequencies for the ν_6, ν_5, ν_4, and ν_3 bands of 7Me-*sw*Mb are slightly shifted from those of native one, reflecting the effect of modification of the heme-propionate side chain in 7Me-*sw*Mb.

Fig.3.2.5 shows the temporal behaviors of intensity changes in the anti-Stokes ν_7 and ν_4 bands for NT- (A), 7Me- (B) and 6 Me-*sw*Mb (C). The temporal changes can be described with a single exponential function as delineated with the solid lines. It is obvious that the intensity decay of ν_7 is slower than that of ν_4, indicating the individual vibrational energy relaxation. The best fit to ν_7 yields the decay constants of 3.4±0.2, 4.9±0.3, and 4.9±0.3 ps for NT-, 7Me- and 6Me-*sw*Mb, respectively (Table 3.2.1). On the other hand, the decay constants of ν_4 are 1.3±0.1, 1.5±0.1, and 1.5±0.1 ps for NT-, 7Me- and 6Me-*sw*Mb, respectively (Table 3.2.1). The comparison

of temporal changes of ν_7 band with normalized intensity for NT- with those for 7Me- and 6Me-swMb is shown in Fig.3.2.5D. The observed decay constants for 7Me- and 6Me-*sw*Mb are extremely close, but are slower by 44% than that of NT-*sw*Mb. This difference is noticeable for ν_7 but less for ν_4. Its reason is not clear but one of plausible interpretations is that ν_4 primarily receives the excess energy and distributes it into other vibrational modes in addition to direct energy flow into the protein matrix. In fact, the rise time of anti-Stokes ν_7 is delayed by 2.5 ps than that of ν_4 for Ni-porphyrin [24], indicating that the intramolecular vibrational energy redistribution (IVR) of porphyrin ring takes place in this time regime. Accordingly, it is likely that the intensity decay of ν_4 of Mb reflects the IVR process of heme, while the intensity decay of ν_7 is mainly determined by the heme-to-solvent intermolecular energy transfer that is significantly delayed by the replacement of the propionate group to the methyl group. Accordingly, small differences in the decay constants of ν_4 among modified hemes are caused by different vibrational mixing between the ν_4 and ν_7 modes of the heme which affects vibrational energy redistribution within the heme. The present observation strongly suggests that the 7- and 6-propionate side chains are responsible for the vibrational energy transfer from heme to the surroundings and thus, the heme "cooling" process is decelerated by the elimination of the propionate side chains. Bu and Straub have studied "cooling" of modified Mb with a "tailored" heme, in which the two propionate side chains are replaced by two hydrogen atoms using molecular dynamics simulation, and they found that the time constant is delayed about 50% compared to the constant of 5.9 ps for NT Mb [4], in qualitative agreement

with the present observation (44%) despite the difference between two kinds of modified hemes. To our knowledge, this is the first observation for appreciable delay of heme cooling induced by selective removal of the propionate side chains.

The propionate side chains are strongly involved in the electrostatic interaction with the polar residues of protein. The 7-propinate is directed to the proximal side of porphyrin plane, and forms hydrogen bonding network with the Leu89, Ser92, His93, and His97 residues, while the 6-propionate is hydrogen bonded with only the Arg45 residue but is connected to a water molecule [25]. In order to know the contribution of these hydrogen bonds in the vibrational energy dissipation of heme, we performed the similar anti-Stokes ps-TR^3 measurements for S92A- and R45L-*sw*Mb, wherein the hydrogen bonding partner of 7- or 6-propionate is site-directedly mutated to Ala or Leu, respectively. The anti-Stokes TR^3 difference spectra of S92A- and R45L-*sw*Mb with time delay from -5 ps to 50 ps are shown as Fig.3.2.6 and 3.2.7. The intensity decay of RR bands occurs in a similar way as native one. The temporal changes of anti-Stokes ν_7 and ν_4 bands obtained with the mutant Mbs are plotted in Fig.3.2.8. Essentially the same intensity decreases as that of NT-*sw*Mb occurs within 10-ps time scale, and the best fit yields the decay constants of 3.8±0.3 (ν_7) and 1.5±0.1 ps (ν_4) for S92A and 3.1±0.2 (ν_7) and 1.3±0.1 ps (ν_4) for R45L, respectively (Table 3.2.1). Distinct from 7Me- and 6Me-*sw*Mb, the two mutants do not largely differ from the native one in the temporal decay of ν_7 and ν_4 bands, indicating the negligible influence of the hydrogen bonding between heme side chains and the apolar residues on the heme "cooling".

The energy "funneling" mechanism was first proposed by Hochstrasser and co-workers [1] and supported later by the simulation results from Sagnella and Straub [2]. Furthermore, they deduced a dominant channel for relaxation of the excess energy as a two-step relaxation process: rapid equipartitioning of energy within the heme followed by the through space collisional energy transfer from the heme side chains to nearby solvating water molecules [2]. Miyata et al. [13] observed the volume expansion of protein moiety with a transient grating technique for deoxyMb following photoexcitation, and concluded that the major part of thermal energy dissipates through protein matrix. This is not inconsistent with the present results, because the energy flow is not limited to ν_7 but occurs through ν_4 and others. It is also noted that both ν_4 and ν_7 are not completely relaxed at 50 ps, implying the presence of slower relaxation process. The significant point of this observation is that the time constant of monopropionate Mb is 4.9 ps, an increase by 44% compared with native one. This demonstrates significant involvement of propionate side chains for the energy dissipation from the vibrationally excited heme to the surrounding environment. Contrastingly, the temporal decays raised from the S92A- and R45L-*sw*Mb are uninfluenced. This result suggests that the rapid energy transfer taking place around 3 ps time regime would be direct to solvent molecules by collision through the propionate side chains rather than to the globin moiety through hydrogen bonding interactions between propionate side chains and apolar residues, and the latter might occur more slowly than that the former [2,26].

References:

1 Henry, E. R., Eaton, W. A., Hochstrasser, R. M. *Proc. Natl. Acad. Sci.* **83** (1986) 8982

2 Sagnella, D. E., Straub, J. E. *J. Phys. Chem. B* **105** (2001) 7057

3 Okazaki, I., Hara, Y., Nagaoka, M. *Chem. Phys. Lett.* **337** (2001) 151

4 Bu, L., Straub, J. E. *J. Phys. Chem. B* **107** (2003) 10634

5 Findsen, E. W., Friedman, J. M., Ondrias, M. R., Simon, S. R. *Science* **229** (1985) 661

6 Janes, S. M., Dalickas, G. A., Eaton, W. A., Hochstrasser, R. M. *Biophys. J.* **54** (1988) 545

7 Lingle, R., Xu, X. B., Zhu, H. P., Yu, S. C., Hopkins, J. B. *J. Phys. Chem.* **95** (1991) 9320

8 Lian, T. Q., Locke, B., Kholodenko, Y., Hochstrasser, R.M. *J. Phys. Chem.* **98** (1994) 11648

9 Lim, M., Jackson, T. A., Anfinrud, P. A. *J. Phys. Chem.* **100** (1996) 12043

10 Mizutani, Y., Kitagawa, T. *Science* **278** (1997) 443

11 Mizutani, Y., Kitagawa, T., *Bull. Chem. Soc. Jpn.* **75** (2002) 623

12 Ye, X., Demidov, A., Rosca, F., Wang, W., Kumar, A., Ionascu, D., Zhu, L., Barrick, D., Wharton, D., Champion, P. M. *J. Phys. Chem. A* **107** (2003) 8156

13 Miyata, R., Terazima, M., *Bull. Chem. Soc. Jpn.* **76** (2003) 1707

14 Mizutani, Y. *J. Chem. Phys.* **109** (1998) 9197

15 Springer, B. A., Egeberg, K. D., Sligar, S. G., Rohlfs, R. J., Mathews, A. J., Olson, J. S. *J. Biol. Chem.* **264** (1989) 3057

16 Hayashi, T., Nakagawa, T., Harada, K., Matsuo, T., Hitomi, Y., Hisaeda, Y. *Chem. Lett.* **33** (2004) 1512

17 Hauksson, J. B. La Mar, G. N. Pandy, R. K.. Rezzano, I. N Smith, K. M. *J. Am. Chem. Soc.* **112** (1990) 6198

18 Schomacker, K. T., Bangcharoenpaurpong, O., Champion, P. M. *J. Chem. Phys.* **80** (1984) 4701

19 Shreve, A. P. Mathies, R. A. *J. Phys. Chem.* **99** (1995) 7285

20 Okamoto, H., Nakabayashi, T., Tasumi, M. *J. Phys. Chem. A* **101** (1997) 3488

21 Abe, M., Kitagawa, T., Kyogoku, Y. *J. Chem. Phys.* **69** (1978) 4526

22 Li, X. Y., Czernuszewicz, R. S., Kincaid, J. R., Stein, P., Spiro, T. G. *J. Phys. Chem.* **94** (1990) 47

23 Nakabayashi, T., Okamoto, H., Tasumi, M. *J. Phys. Chem. A* **101** (1997) 3494

24 Y. Mizutani, Y. Uesugi, T. Kitagawa, J. Chem. Phys. 111 (1999) 8950.

25 Kachalova, G. S., Popov, A. N., Bartunik, H. D. *Science* **284** (1999) 473

26 Mizutani, Y., Kitagawa, T. *J. Phys. Chem. B* **105** (2001) 10992

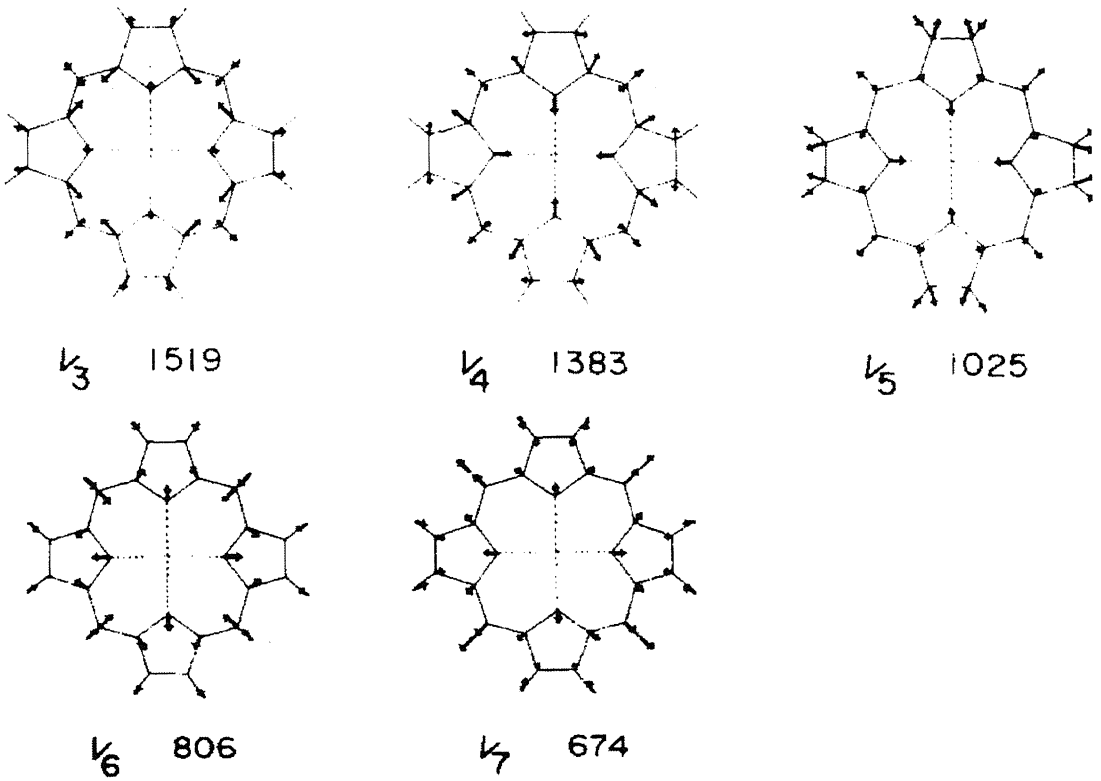

Fig.3.2.1 Displacement vectors of some vibrational modes of octaethyl phorphyrinato-Ni(II) [Ni(OEP)] (taken from ref.21).

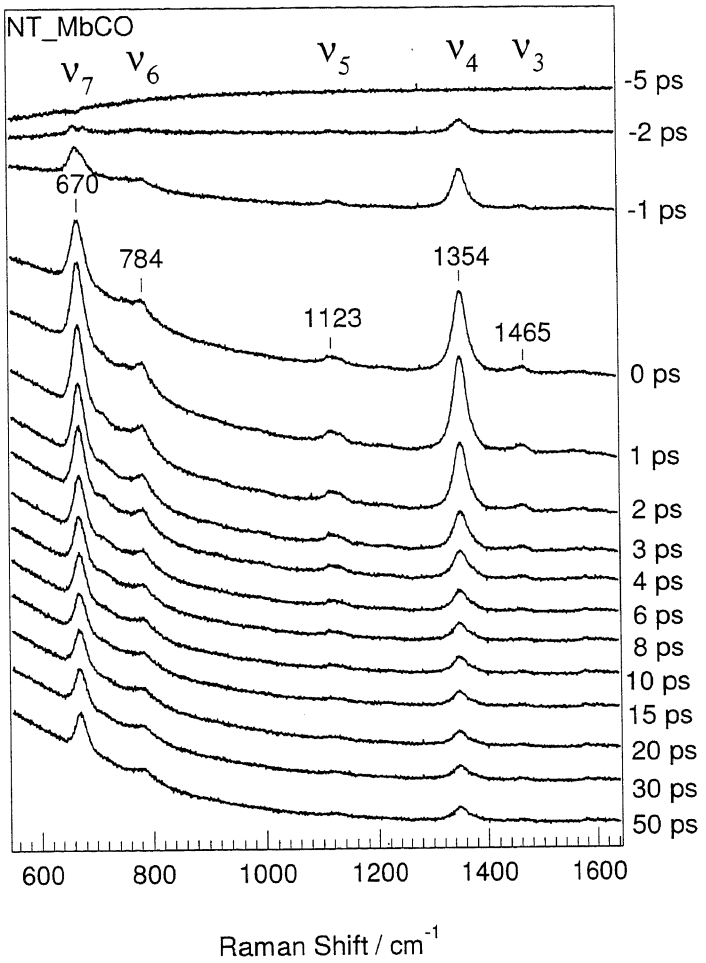

Fig.3.2.2. TR^3 anti-Stokes spectra of photodissociated MbCO for the time delays from-5 to 50 ps in the 600 to 1600 cm^{-1} region for NT-*sw*Mb. The spectra are represented as difference spectra relative to the probe-only spectrum.

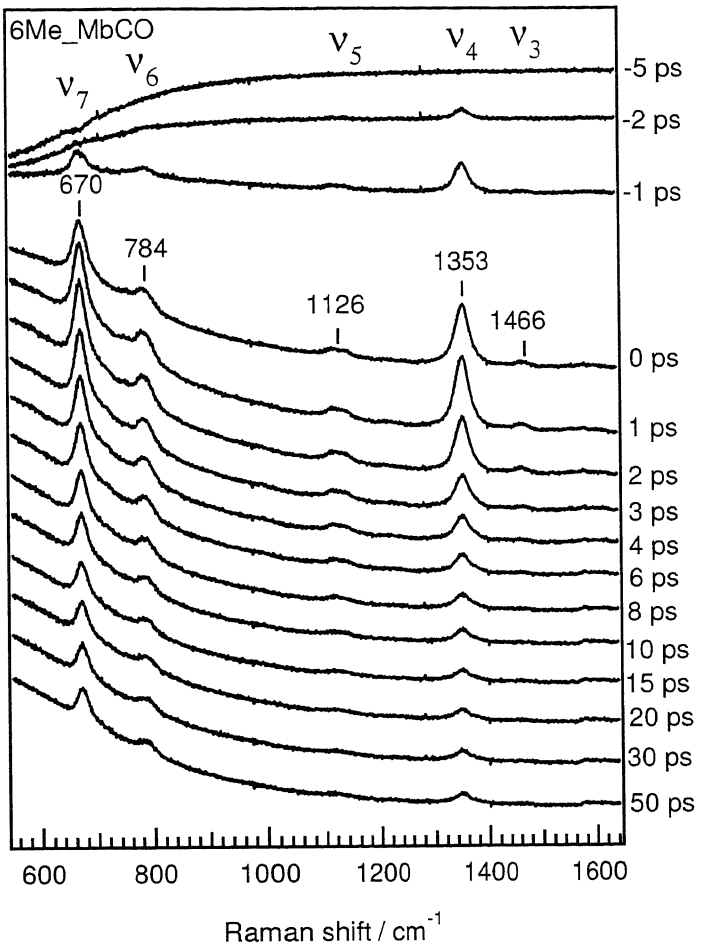

Fig.3.2.3. TR^3 anti-Stokes spectra of photodissociated MbCO for the time delays from-5 to 50 ps in the 600 to 1600 cm^{-1} region for 6Me-*sw*Mb. The spectra are represented as difference spectra relative to the probe-only spectrum.

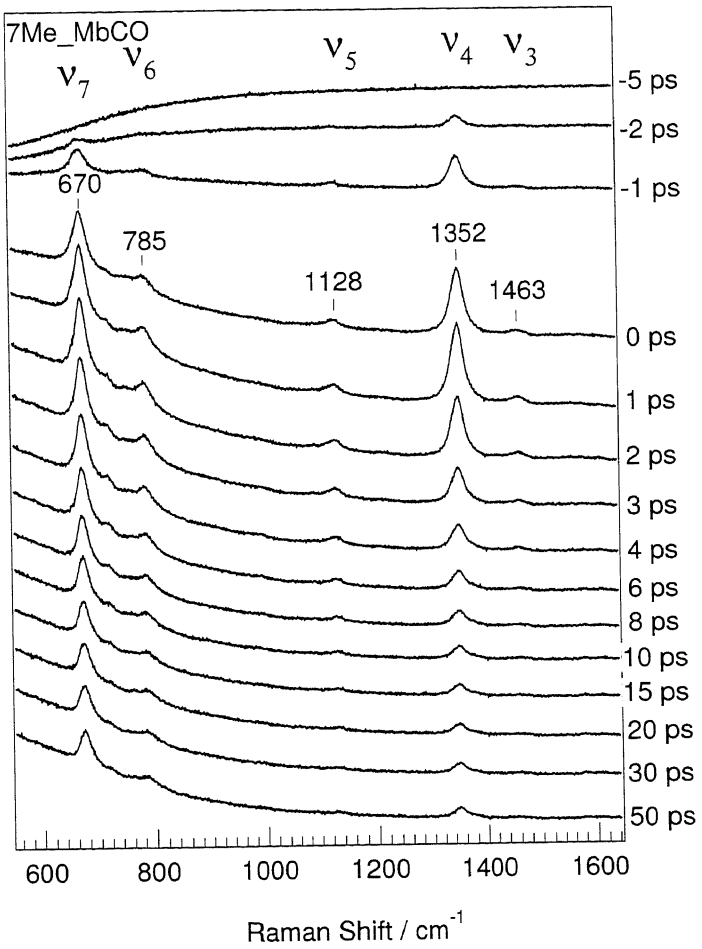

Fig.3.2.4. TR^3 anti-Stokes spectra of photodissociated MbCO for the time delays from-5 to 50 ps in the 600 to 1600 cm^{-1} region for 7Me-*sw*Mb. The spectra are represented as difference spectra relative to the probe-only spectrum.

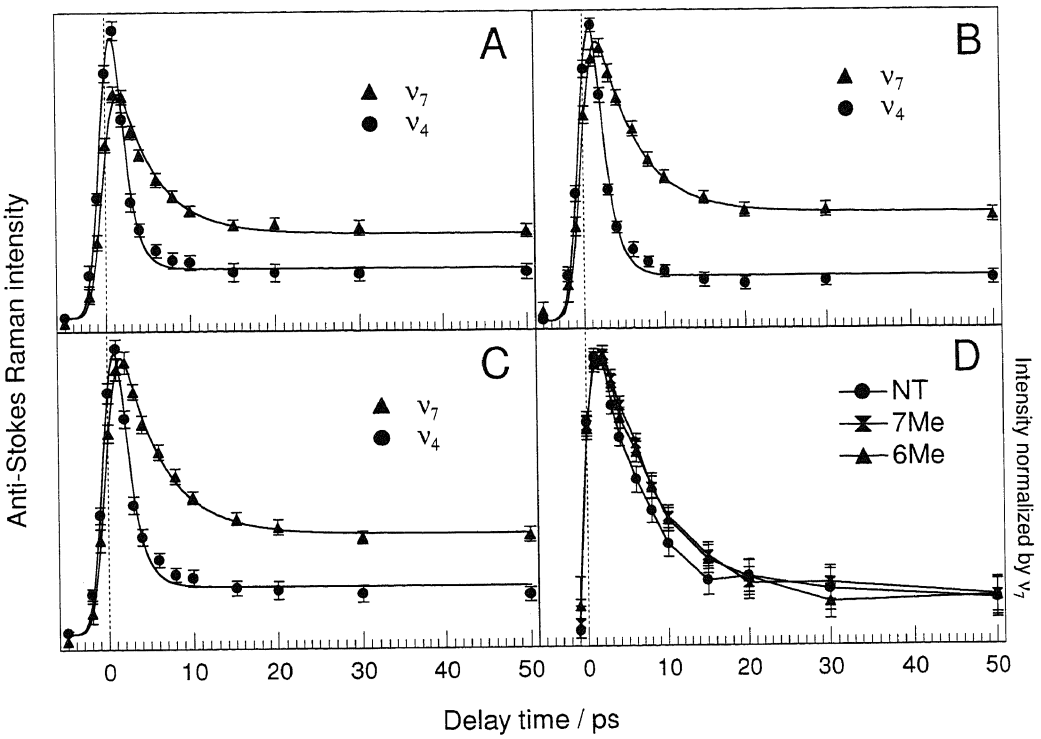

Fig.3.2.5. Temporal changes of the Raman intensity of the anti-Stokes ν_7 (▲) and ν_4 bands (●) of photodissociated MbCO. (A) NT-*sw*Mb, (B) 7Me-*sw*Mb, (C) 6Me-*sw*Mb, and (D) Superimposition of ν_7 band for NT-, 7Me-, and 6Me-*sw*Mb with normalized Raman intensities. The solid lines are best fit to an exponential decay ($A[\exp(-t/\tau_{decay})+B]$) convoluted with the instrument response function.

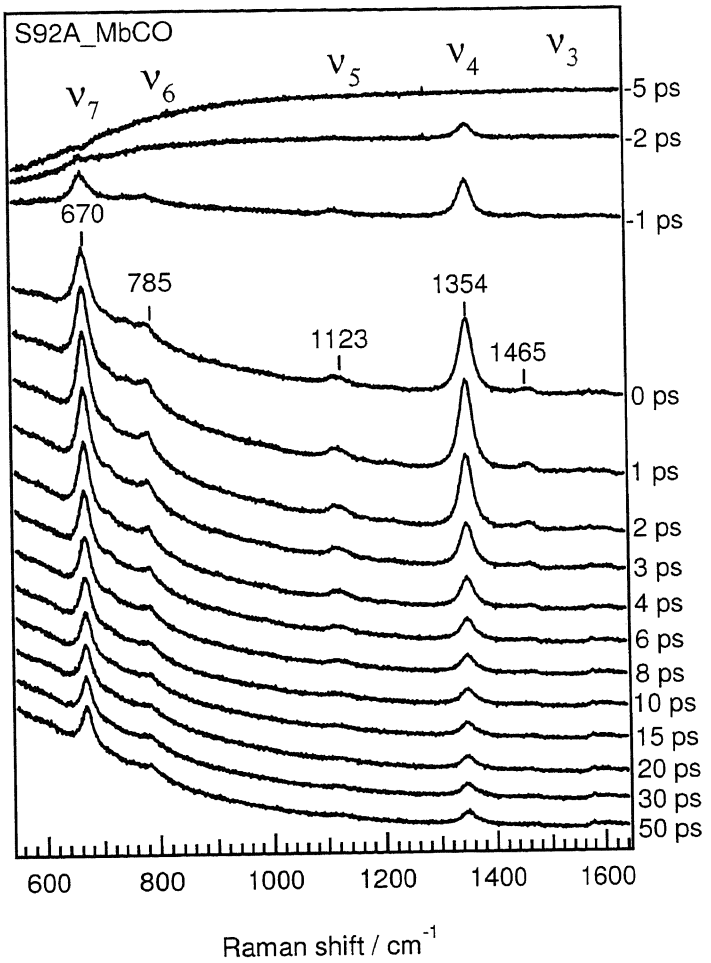

Fig.3.2.6. TR^3 anti-Stokes spectra of photodissociated MbCO for the time delays from-5 to 50 ps in the 600 to 1600 cm^{-1} region for S92A-*sw*Mb. The spectra are represented as difference spectra relative to the probe-only spectrum.

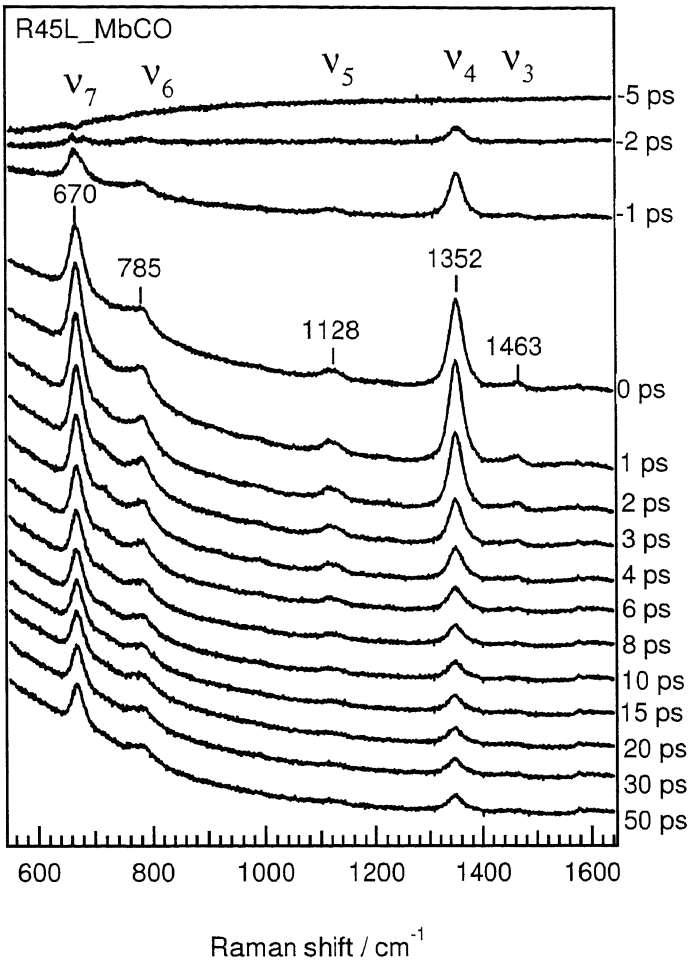

Fig.3.2.7. TR^3 anti-Stokes spectra of photodissociated MbCO for the time delays from-5 to 50 ps in the 600 to 1600 cm^{-1} region for R45L-*sw*Mb. The spectra are represented as difference spectra relative to the probe-only spectrum.

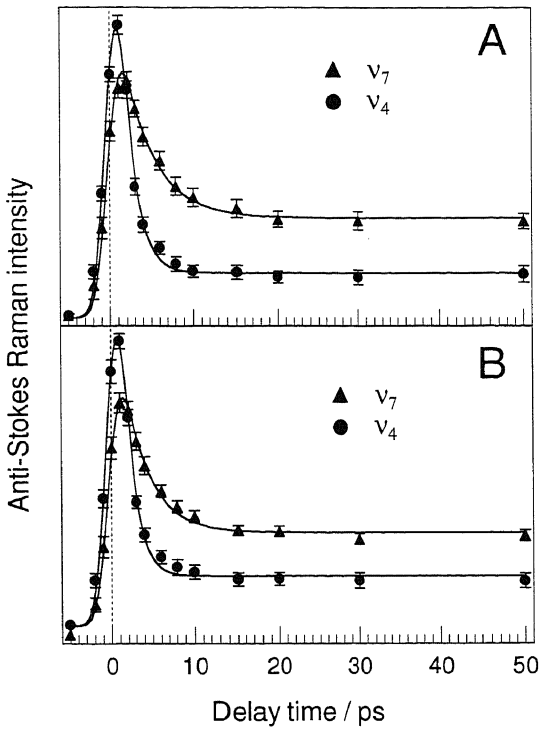

Fig.3.2.8. Temporal changes of the Raman intensity of the anti-Stokes ν_7 (▲) and ν_4 bands (●) of photodissociated MbCO. (A) S92A-*sw*Mb, (B) R45L-*sw*Mb. The solid lines are best fit to an exponential decay ($A[\exp(-t/\tau_{decay})+B]$) convoluted with the instrument response function.

Table 3.2.1. Time Constants for Intensity Changes of the ν_7 and ν_4 Anti-Stokes Raman Bands of *sw*Mb Samples.

Mbs	**ν_7 / ps**	**ν_4 / ps**
NT	3.4±0.2	1.3±0.1
7Me	4.9±0.3	1.5±0.1
6Me	4.9±0.3	1.5±0.1
S92A	3.8±0.3	1.5±0.1
R45L	3.1±0.2	1.3±0.1

Chapter 4. General Conclusion

Conclusion

In this study, the interactions between heme and protein matrix as well as solvent leading to in intramolecular transduction of structural information and intermolecular energy transfer were systematically investigated by using Mb. Those interactions include the covalent bond and the hydrogen bonds between heme and globin and spatial collision between heme side chains and water molecules.

In order to investigate the transmission of a binding signal of a gaseous ligand from the ligand binding site—heme, to protein moiety in gas sensory heme proteins, we applied UVRR spectroscopy to myoglobin as a model. UVRR spectroscopy is known as an excellent tool for monitoring protein conformational changes. First of all, we determined the changes of conformation in globin that occur upon binding of CO, NO, or O_2 to heme. Specifically, NO induces spectral changes in Trp residues of A-helix that are significantly different from those induced by O_2 or CO binding. On the other hand, binding of O_2 to heme produces spectral changes in the Tyr residues of H-helix that are different from those induced by CO or NO binding. The UVRR results demonstrate that the heme discriminates among different ligands by driving corresponding conformational changes in the globin matrix. In order to explore the signaling pathway through His93 covalent bond, and 6- or 7-propionate hydrogen bonding network, we extended measurements to mutant- and heme-modified Mbs in a similar way to native Mb, and investigated how they are responsible for transmitting structural changes from ligand binding site--heme to globin for different ligands. As shown in Fig.4.1, the experimental results demonstrate that the cleavage of Fe-His93

covalent bond eliminates communication to the C-terminal of the H-helix and that 7-propionate hydrogen-bonding network is essential for transmitting the CO or NO binding signal to the N- and C-termini. Finally, 6-propionate is important only for NO binding. Thus, the hydrogen-bonding network in the protein appears to be critical for intramolecular signal transduction in gas sensory heme proteins.

Furthermore, pathway of vibrational energy dissipation from the heme to surrounding protein matrix and solvent following CO photolysis in the fast time component ($\leq$ 10 ps) was investigated by using picosecond time-resolved anti-Stokes Raman spectroscopy. The modified- and mutant Mbs, in which the 6- or 7-propionate is selectively replaced by a methyl group or related hydrogen bonds is eliminated by mutagenesis was used as model systems. The time constants of population decay of vibrationally excited states for two modified Mbs became significantly larger compared with those of native Mb. However the corresponding values of mutants are not different from those of the native Mb. As shown in Fig.4.2, this work indicates that the two heme-propionate side chains are highly involved in the energy transfer from the heme to solvent through the collision with surrounding water molecules and contribute equally. But the hydrogen bonding interactions with protein matrix seem to contribute scarcely to this fast energy transfer process. This is the first experimental data estimating the contribution of individual heme-propionate side chains to the vibrational energy transfer from the heme to the surroundings.

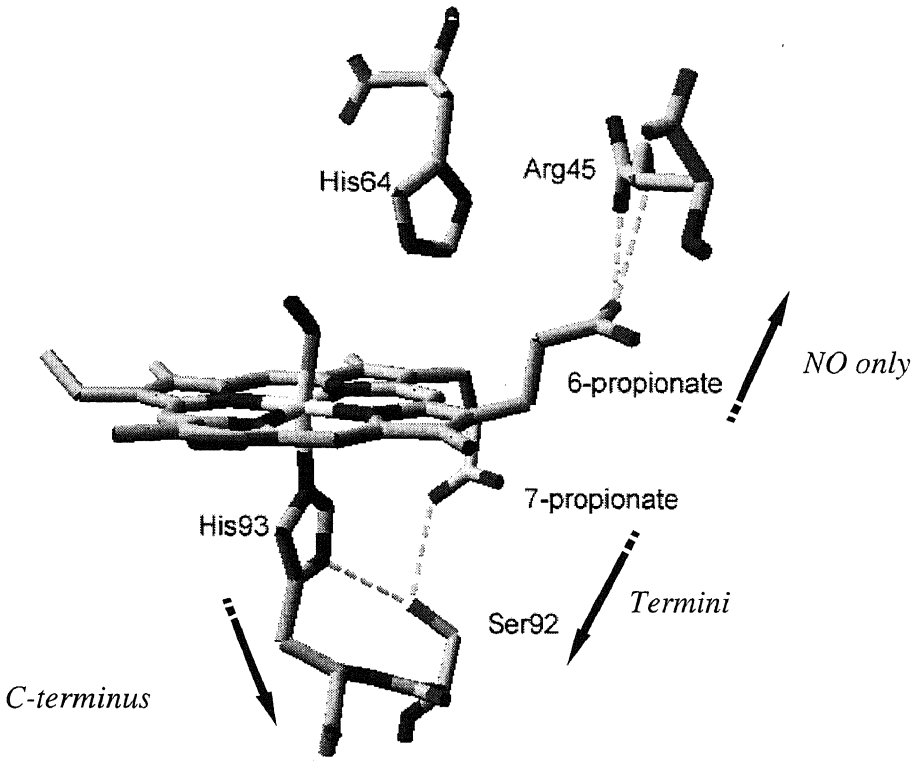

Fig.4.1 Scheme for structural information transmission in Mb. Arrow indicates the pathways for transmission.

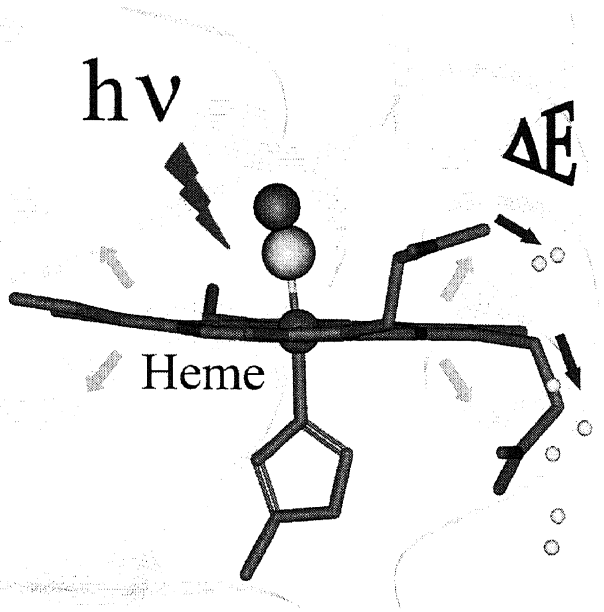

Fig.4.2 Scheme for vibrational energy transfer in Mb following CO photolysis. Arrow indicates the pathways for energy dissipation.

Appendix: Visible RR Data of Heme-modified Mb Compared with Native Mb

Visible RR data of native Mb, and heme-modified reconstituted Mbs (7M6P and 6M7P) was collected here (Fig.A1-2). This set of measurements is useful to compare the mono-propionate heme structures in modified Mbs with the normal heme structure in native one. Also it is used as an identification of the correct cooperation between the synthesized heme and apo-Mb (as refered in section 2.2.3 and 3.2.3). Because the vibrational modes of Fe-His stretching (Fig.A1, 219 cm^{-1}) and Fe-CO stretching (Fig.A2, 508 cm^{-1}) and bending mode (Fig.A2, 577 cm^{-1}) can be regarded as marker bands for the correct cooperation. Raman modes of native Mb, 7M6P and 6M7P were summarized in Table A1 and A2. The assignment of vibrations is according to the report of Abe M. et al [1].

References:

1. Abe, M., Kitagawa, T., and Kyogoku, Y. (1978) *J. Chem. Phys.* **69**, 4526

Table A1. Visible RR data of deoxy form NT-, 7M6P- and 6M7P-swMb.

Numbers	NT/ cm^{-1}	7M6P/ cm^{-1}	6M7P/ cm^{-1}	Assignment [1]
ν(Fe-His)	219.0	219.4	218.5	Fe-His streching
ν_9	239	250	238	C_β-C_1 bending,mainly involves 6,7 propionate groups and 5,8 methyl groups
γ_7	302	300	302	methine wagging
γ_6	334	336	338	pyrrole tilting
ν_8	342	344	346	νM-N
$\delta(C_\beta C_c C_d)$	370	375	382	porphyrin-propionate bending
$\delta(C_\beta C_a C_b)$	405	403	404	porphyrin-vinyl bending
$\delta(C_\beta C_a C_b)$	436		434	porphyrin-vinyl bending
γ_{12}	499	489/499	485	pyrrole swiveling
γ_{21}	544	546	543	pyrrole folding
ν_{48}	585		582/593	pyrrole deform,symmetric
ν_7	673	675	673	pyrrole deform,symmetric
γ_{11}	720	723	721	pyrrole folding
γ_5	734		733	pyrrole folding
ν_{15}	758	756	759	pyrrole breathing
ν_{47}	778	781	783	pyrrole breathing
ν_8	789	789	793	νM-N

Table A2. Visible RR data of CO-bound form NT-, 7M6P- and 6M7P-swMb.

Numbers	NT /cm^{-1}	7M6P/ cm^{-1}	6M7P/ cm^{-1}	Assignment [1]
ν_9	253	259	249	C_β-C_1bending,mainly involves 6,7 propionate groups and 5,8 methyl groups
γ_{16}	318	317	309	pyrrole tilting
ν_8	346	344	344	νM-N
$\delta(C_\beta C_c C_d)$	379	382	382	porphyrin-propionate bending
$\delta(C_\beta C_a C_b)$	411	410	410	porphyrin-vinyl bending
$\delta(C_\beta C_a C_b)$	438	429	435	porphyrin-vinyl bending
ν(Fe-CO)	507.7	508.4	506.3	Fe-C stretching
δ(Fe-CO)	576/584	577	576	Fe-C bending
ν_7	675	676	675	pyrrole deform,symmetric
γ_{11}	719	718	720	pyrrole folding
γ_5	733	724	734	pyrrole folding
ν_{15}	755	755	755	pyrrole breathing

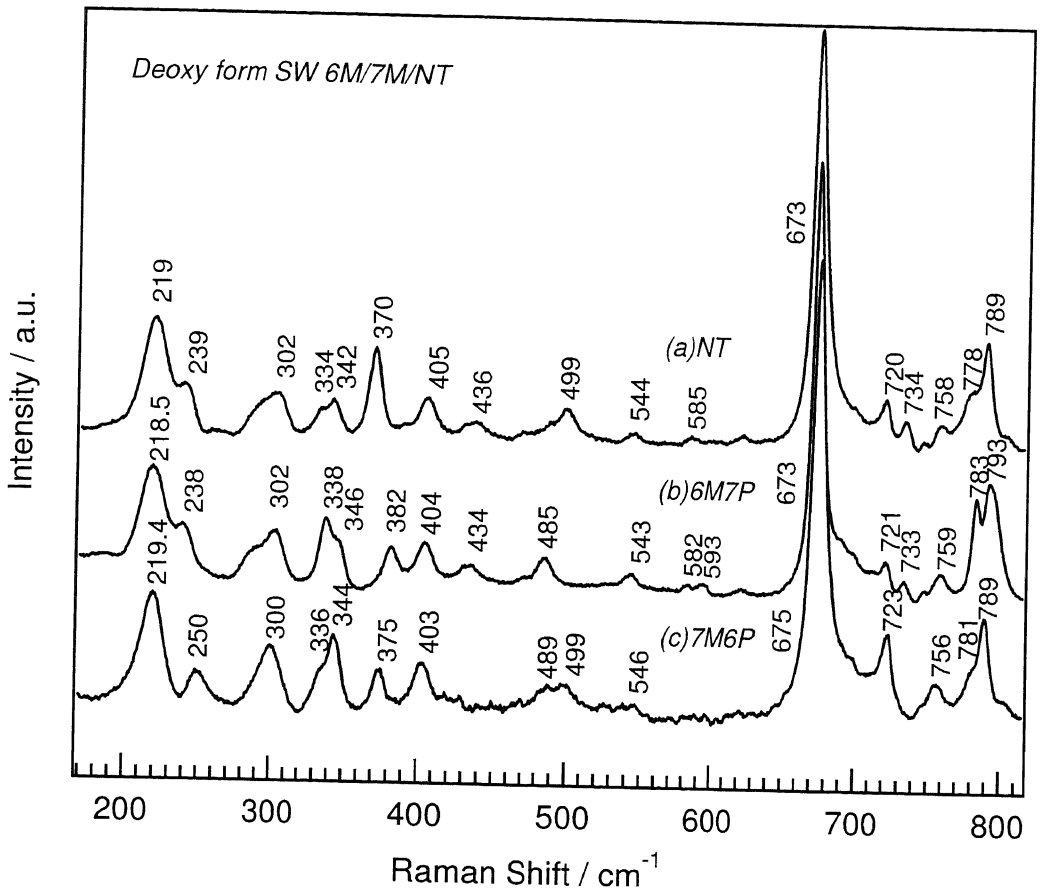

Fig.A1. Visible RR spectra of deoxy form NT-, 7M6P- and 6M7P-swMb at excitation wavelength of 427.8 nm, 35 mM protein solution in 50 mM phosphate buffer at pH 7.0.

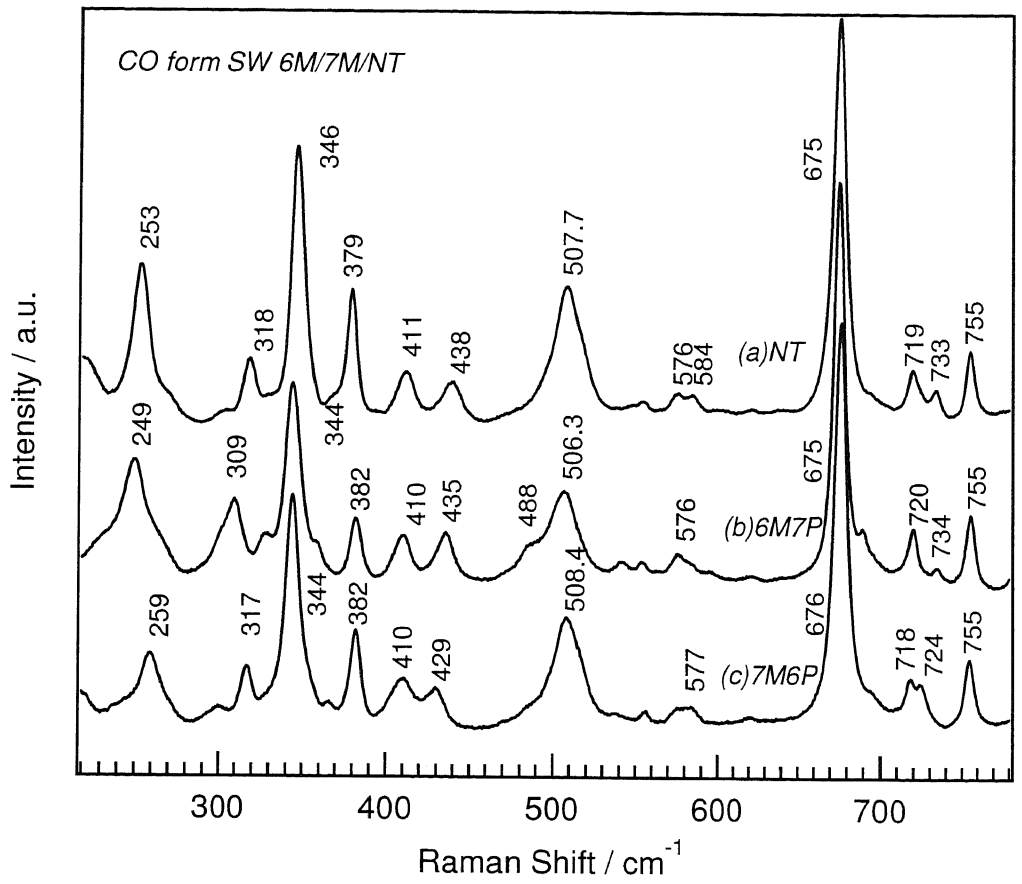

Fig.A2. Visible RR spectra of CO-bound form NT-, 7M6P- and 6M7P-swMb at excitation wavelength of 427.8 nm, 35 mM protein solution in 50 mM phosphate buffer at pH 7.0.

Abbreviations

(Alphabetically arranged)

6M7P	reconstituted myoglobin with modified heme in which 6-propionate is replaced by a methyl group
7M6P	reconstituted myoglobin with modified heme in which 7-propionate is replaced by a methyl group
*Bj*FixLH	Bradyrhizobium japonicum FixL heme-binding domain
cAMP	cyclic adenosine 3',5'-monophosphate
cGMP	cyclic 3',5'-guanosine monophosphate
CO-bound Mb	MbCO
deoxyHb	deoxy state of hemoglobin
deoxyMb	deoxy form of myoglobin
*Ec*DOS	direct oxygen sensor from *Escherichia coli*
*Ec*DOSH	*Ec*DOS heme-binding domain
GTP	5'-guanosine triphosphate
Hb	hemoglobin
HemAT	heme-based aeroxtaxis transducer
*h*Mb	horse myoglobin
Imd	Imidazole
Mb	myoglobin
Ni(OEP)	octaethyl phorphyrinato-Ni(II)
NT	native
OPA	Optical parametric amplifier
OPG	Optical parametric generator
PAS	Per-Arnt-Sim
ps-TR^3	picosecond-TR^3
relaxed	R
rmsd	root-mean-square deviation
RR	Resonance Raman
sGC	Soluble guanylate cyclase
*sw*Mb	sperm whale myoglobin
tense	T
TR^3	Time-resolved resonance Raman
UVRR	Ultraviolet resonance Raman
YC-1	3-(5'-hydroxymethly-2'-furyl)-1-benzylindazole

List of Publication

1. Gao Y., El-Mashtoly S. F., Pal B., Hayashi T., Harada K., Kitagawa T., Pathway of Information Transmission from Heme to Protein upon Ligand Binding/Dissociation in Myoglobin Revealed by UV Resonance Raman Spectroscopy. *J. Biol. Chem.* **281** (34), 24637-24646, 2006.

2. Gao Y., El-Mashtoly S. F. Pal B., Hayashi T., Harada K., Kitagawa T., Signal Transfer Mechanisms from Heme to Protein in Myoglobin. *J. Porphyr. Phthalocyanines* Accepted in May, 2006.

3. Gao Y., Koyama M, El-Mashtoly S. F., Hayashi T., Harada K., Mizutani Y. and Kitagawa T., Time-resolved Raman Evidence for Energy "Funneling" through Propionate Side Chains in Heme "Cooling" upon Photolysis of Carbonmonoxy Myoglobin. *Chem. Phys. Lett.* 429 (1-3), 239-243, 2006.

4. Sato A., Gao Y., Kitagawa T. and Mizutani Y., Site-specific Observation of Ultrafast Structural Relaxation of Photodissociated Carbonmonoxy Myoglobin. Soon will be submitted to *J. Phys. Chem. B*

Acknowledgement

This thesis summarized the author's doctoral studies from 2003 to 2006 at the department of Photoscience, the Graduate University for Advanced studies. The experiment has been performed in Okazaki Institute for Integrative Bioscience, National Institutes of Natural Sciences. The author would appreciate sincerely for the guidance of her supervisor, Prof. Teizo Kitagawa. His patience, encouragement, criticism is indispensable for the author to achieve her studies. The author is also grateful to Dr. Samir F. El-Mashtoly for his helpful discussion and kind advice of ultraviolet resonance Raman spectroscopy. The author also owes Dr. Biswajit Pal for his introducing of biochemical works.

The author would thanks greatly to Prof. Takashi Hayashi and Dr. Katsuyoshi Harada (Osaka Univ.) for their kindly supporting of the synthesized modified hemin used in this study.

The ps-TR^3 anti-Stokes experiments could not be performed without the great help of Prof. Yasuhisa Mizutani (Osaka Univ.) and Ms. Mai Koyama (Kobe Univ.). The author appreciates deeply for them as well as the cooperation of Dr. Akira Sato (Kobe Univ.).

The author would express acknowledgments for all the members in Kitagawa Lab., Dr. Takeshi Uchida, Takehiko Tosha, Hirotsugu Hiramatsu, Takehiro Ohta, Minoru Kubo, Prof. Satoru Nakashima, Dr. Konstantinos Koutsoupakis, Prof. Yuzong Gu and the other doctoral students Jiang Li and Ming Lv, for their valuable discussion

and kindly help for her study. The author also wishes to thank the kindness and official support for Ms. Miho Isogai and Hiroko Mizuki.

Finally, the author thanks her families for their constant understanding and encouragement.

June, 2006

Okazaki

Ying Gao